

Alma Mater Studiorum Università di Bologna
Archivio istituzionale della ricerca

INPP4B overexpression and c-KIT downregulation in human achalasia.

This is the final peer-reviewed author's accepted manuscript (postprint) of the following publication:

Published Version:

E. Bonora, F.B. (2018). INPP4B overexpression and c-KIT downregulation in human achalasia. *NEUROGASTROENTEROLOGY & MOTILITY*, 30(9), 1-13 [10.1111/nmo.13346].

Availability:

This version is available at: <https://hdl.handle.net/11585/653766> since: 2021-01-29

Published:

DOI: <http://doi.org/10.1111/nmo.13346>

Terms of use:

Some rights reserved. The terms and conditions for the reuse of this version of the manuscript are specified in the publishing policy. For all terms of use and more information see the publisher's website.

This item was downloaded from IRIS Università di Bologna (<https://cris.unibo.it/>).
When citing, please refer to the published version.

(Article begins on next page)



INPP4B overexpression and c-KIT downregulation in human achalasia

Journal:	<i>Neurogastroenterology and Motility</i>
Manuscript ID	NMO-00426-2017.R1
Manuscript Type:	Original Article
Date Submitted by the Author:	n/a
Complete List of Authors:	<p>Bonora, Elena; Medical Genetics Unit, St.Orsola Malpighi Bianco, Francesca; University of Bologna Stanzani, Agnese; University of Bologna, Medical and Surgical Sciences Giancola, Fiorella; University of Bologna, Department of Veterinary Medical Sciences Astolfi, Annalisa; University of Bologna, Medical and Surgical Sciences Indio, Valentina; University of Bologna, Medical and Surgical Sciences Evangelisti, Cecilia Martelli, Alberto; University of Bologna, DIBINEM Boschetti, Elisa; University of Bologna, Medical and Surgical Sciences Lugaresi, Marialuisa; University of Bologna, Medical and Surgical Sciences Ioannou, Alexandros; University of Bologna, Medical and Surgical Sciences Torresan, Francesco Stanghellini, Vincenzo Clavenzani, Paolo Seri, Marco; Medical Genetics Unit, St.Orsola Malpighi Moonen, An van Beek, Kim; KU Leuven Wouters, Mira M.; Katholieke Universiteit Leuven Faculteit Wetenschappen, Translational Research in Gastrointestin Boeckxstaens, Guy; KUL, Zaninotto, Giovanni Mattioli, Sandro; University of Bologna, Medical and Surgical Sciences De Giorgio, Roberto; University of Bologna, Medical and Surgical Sciences</p>
Key Words:	Achalasia, c-Kit, INPP4B, transcriptome, cell signaling

1
2
3
4
5
6
7
8
9
10
11
12
13
14
15
16
17
18
19
20
21
22
23
24
25
26
27
28
29
30
31
32
33
34
35
36
37
38
39
40
41
42
43
44
45
46
47
48
49
50
51
52
53
54
55
56
57
58
59
60

***INPP4B* overexpression and *c-KIT* downregulation in human achalasia**

***Running title:* INPP4B and c-KIT dysregulation in achalasia**

Elena Bonora¹, Francesca Bianco^{1,2}, Agnese Stanzani^{1,2}, Fiorella Giancola^{1,2,3},
Annalisa Astolfi⁴, Valentina Indio⁴, Cecilia Evangelisti⁵, Alberto Maria Martelli⁵,
Elisa Boschetti^{1,3}, Marialuisa Lugaresi¹, Alexandros Ioannou¹, Francesco Torresan⁶,
Vincenzo Stanghellini¹, Paolo Clavenzani², Marco Seri¹, An Moonen⁷, Kim Van
Beek⁷, Mira Wouters⁷, Guy E. Boeckxstaens⁷, Giovanni Zaninotto⁸, Sandro Mattioli¹
and Roberto De Giorgio⁹

¹ Department of Medical and Surgical Sciences, DIMEC, University of Bologna and St. Orsola-Malpighi Hospital, Bologna, Italy.

² Department of Medical and Veterinary Sciences, DIMEVET, University of Bologna, Bologna, Italy.

³ Centro di Ricerca Biomedica Applicata, St.Orsola-Malpighi Hospital, Bologna, Italy

⁴ Interdepartmental Center for Cancer Research “G. Prodi” (CIRC), University of Bologna, Bologna, Italy.

⁵ Department of Experimental Medicine, DIMES, University of Bologna, Bologna, Italy.

⁶ Department of Digestive System, St. Orsola-Malpighi Hospital, Bologna, Italy.

⁷ Translational Research in GastroIntestinal Disorders (TARGID), Department of Clinical and Experimental Medicine, KU Leuven University, Belgium.

⁸ Division of Surgery, Imperial College London, London, United Kingdom.

⁹ Department of Medical Sciences, Nuovo Arcispedale S. Anna at Cona (Ferrara),
University of Ferrara, Italy.

Funding

FB is recipient of a Telethon fellowship. This work was supported by grant
GGP15171 from Fondazione Telethon and University of Bologna (RFO funds) to EB
and RDeG. RDeG received research grants from Fondazione Del Monte of Bologna
and Ravenna. The funding bodies did not influence the content of this article.

Abbreviations

CPM - count per million, GO - gene ontology, LES - lower esophageal sphincter,
MEV - multiple experiment viewer, ICC - interstitial cells of Cajal, INPP4B - inositol
polyphosphate-4-phosphatase, type II B.

Correspondence address:

Roberto De Giorgio, MD, PhD, AGAF

Department of Medical Sciences,

University of Ferrara, Ferrara, Italy

e-mail: deg@aosp.bo.it

Tel.: +39-0532688156

Fax: +39-0532688156

Conflict of interest

The authors declare no conflict of interest

Author contribution

EB, RDeG conceived the study, performed data analysis and wrote the manuscript; AA, FB, VI, performed RNAseq and data analysis; AS, VB, FG, KVB, CE, EB performed immunostaining and western blotting analysis; ML, AI, FT, GZ; AM, MW, GEB, SM provided the clinical cases and tissue biopsies; SM, EB, RDeG, GEB, MS, VS performed critical revision of the manuscript. All authors read the final version of the paper.

Key points

- Primary achalasia is a disorder due to neuronal defects supplying the esophagus leading to altered peristalsis and lack of sphincter relaxation. Nonetheless, the molecular mechanisms involved in this condition are poorly understood.
- Transcriptomic analysis of achalasic tissues identified a dysregulated expression of different genes, in particular c-KIT (downregulated) and INPP4B (upregulated), the latter being linked to Akt pathway regulation.
- Our results unravel novel signaling pathways involved in the neuronal and interstitial cells of Cajal abnormalities in primary achalasia.

Abstract

Background & Aims: Achalasia is a rare motility disorder characterized by myenteric neuron and interstitial cells of Cajal (ICC) abnormalities leading to deranged/absent peristalsis and lack of relaxation of the lower esophageal sphincter. The mechanisms contributing to neuronal and ICC changes in achalasia are only partially understood. Our goal was to identify novel molecular features occurring in patients with primary achalasia.

Methods: Esophageal full-thickness biopsies from 42 (22 females; age range: 16-82 yrs) clinically, radiologically and manometrically characterized patients with primary achalasia were examined and compared to those obtained from ten subjects (controls) undergoing surgery for uncomplicated esophageal cancer (or upper stomach disorders). Tissue RNA extracted from biopsies of cases and controls was used for library preparation and sequencing. Data analysis was performed with the 'edgeR' option of R-Bioconductor. Data were validated by real-time RT-PCR, western blotting and immunohistochemistry.

Key Results: Quantitative transcriptome evaluation and cluster analysis revealed 111 differentially expressed genes, with a $P \leq 10^{-3}$. Nine genes with a $P \leq 10^{-4}$ were further validated. *CYR61*, *CTGF*, *c-KIT*, *DUSP5*, *EGR1* were downregulated, whereas *AKAP6* and *INPP4B* were upregulated in patients vs controls. Compared to controls, immunohistochemical analysis revealed a clear increase in INPP4B, whereas c-KIT immunolabeling resulted downregulated. Since INPP4B regulates Akt pathway, we used western blot to show that phospho-Akt was significantly reduced in achalasia patients vs controls.

Conclusions & Inferences: The identification of altered gene expression, including *INPP4B*, a regulator of the Akt pathway, highlights novel signaling pathways involved in the neuronal and ICC changes underlying primary achalasia.

Key words: Achalasia, cell signaling, c-KIT, *INPP4B*, transcriptome.

For Peer Review

109 Introduction

110 Achalasia is a primary motility disorder of the esophagus occurring at any age, with
111 an estimated annual incidence of approximately 0.03-1 per 100 people and affecting
112 both sexes equally.^{1,2} Achalasia can be classified into primary forms (mostly
113 idiopathic), and cases associated with systemic disorders.^{3,4} From a pathogenetic
114 stand-point, achalasia is characterized by a predominant loss of inhibitory myenteric
115 neurons with a relative increase of cholinergic motoneurons⁵. Progressively
116 degenerative processes may involve virtually all neurons over time. These neuronal
117 changes result in an increase of the lower esophageal sphincter (LES) tone, which, in
118 conjunction with an altered peristalsis of the esophageal body, represent the
119 manometric correlate of any form of achalasia.⁶ Because of these functional
120 abnormalities patients with achalasia complain of dysphagia, regurgitation and chest
121 pain, often severe enough to require either surgery or pneumatic dilatation⁷.
122 Mechanisms leading to esophageal myenteric neurodegeneration and loss include
123 autoimmune responses likely triggered by environmental factors (e.g., neurotropic
124 viruses) in genetically predisposed individuals.^{2,3,8} In addition to neurons,
125 abnormalities of interstitial cells of Cajal (ICC), the pace-maker cells of the
126 gastrointestinal tract, were demonstrated in patients with achalasia⁹.

127
128 The current standard for diagnosing achalasia is high-resolution manometry, although
129 molecular biomarkers would be useful not only for diagnostic purposes, but also to
130 address targeted therapeutic options so far not yet available. Proteomic analysis of
131 sera from patients with achalasia and healthy individuals showed disease-related
132 upregulation of transthyretin (TTR), a carrier of thyroid hormone thyroxine and a
133 retinol-binding protein, associated with familial amyloid polyneuropathy.¹⁰ The

134 observed upregulation may correlate with the consequent neural degeneration
135 observed in achalasic patients.¹¹ Other studies demonstrated increased deposits of the
136 complement complex C5b-C9 and IgM within or proximal to ganglion cells of the
137 esophageal myenteric plexus.¹²

138 Achalasia due to rare genetic abnormalities includes recessive forms with mutations
139 in the neuronal nitric oxide synthase gene, *NOS1*¹³, or in *ALADIN* gene¹⁴ (Allgrove
140 syndrome or triple A syndrome, characterized by alacrima, achalasia and adrenal
141 cortex failure; OMIM #231550). Genome-wide and candidate gene association
142 studies have implicated the human leukocyte antigen (HLA) class II system as the
143 underlying genetic predisposing factor in achalasia. In particular, an 8-residues
144 insertion in the cytoplasmic tail of HLA-DQB1 has been identified as a strong risk
145 factor for achalasia, with a specific geospatial north-south gradient among
146 Europeans.¹⁵ Two amino acid substitutions in the extracellular domain of HLA-
147 DQα1, (lysine 41 encoded by HLA-DQA1*01:03) and of HLA-DQB1, (glutamic acid
148 45, encoded by HLA-DQB1*03:01 and HLA-DQB1*03:04) were characterized as
149 independent risk factors for achalasia and patients with the DQA1*0103 and
150 DQB1*0603 alleles have a significantly higher prevalence of anti-myenteric
151 antibodies.¹⁵⁻²⁰

152 Nevertheless, the mechanisms contributing to the observed neuronal and ICC changes
153 in achalasia are still partially understood. The aim of this study was to identify the
154 dysregulated molecular pathways / events occurring in primary (idiopathic) achalasia
155 to provide a molecular signature of primary achalasia.

157 **Materials and Methods**

158 **Patients and tissue biopsies**

A number of 42 (n= 20 from Italy; n= 22 from Belgium; 22 females; age range: 16-82 yrs) patients with a well-established clinical, radiological and manometric diagnosis of primary achalasia were recruited (Supplementary Table 1A). The included patients were all of Caucasian origin. Each patient underwent surgery and 1-2 tissue samples were obtained via a laparoscopic extramucosal Heller's myotomy extended 4-5 cm along the distal esophagus (i.e., 1-2 cm full-thickness biopsy containing the circular and longitudinal muscle with the associated enteric nervous system). Comparable control tissues were obtained from the corresponding esophageal region of 10 (3 females; age range: 45-87 yrs) controls, who were referred to surgery for uncomplicated esophageal cancer and upper stomach disorders, as reported in Supplementary Table 1B. Margins of all of sampled tissues were free of cancer. Signed informed consent was obtained for each subject enrolled in the study and data handling was performed according to the Helsinki declaration. The study was approved by the local Ethic Committee (study 42/2011/0/Oss protocol #877/211).

RNA extraction

Total RNA was extracted with the RiboPure kit from fresh frozen biopsies stored at -80°C in RNAlater, according to the manufacturer's instruction (Ambion, ThermoFisher Scientific, Waltham, MA, USA). RNA was resuspended in 40 µl of RNase-free water, and quality and quantity of RNA were evaluated on Agilent Bioanalyzer 2100 instrument (Agilent, Santa Clara, CA, USA). 150 ng of RNA was used for each library preparation, according to the TruSeq RNA Sample Prep v2 protocol (Illumina, San Diego, CA, USA). Poly(A)-RNA molecules from 500 ng of total RNA were purified using oligo-dT magnetic beads. Following purification, the mRNA was fragmented and randomly primed for reverse transcription followed by second-strand synthesis to create double-stranded cDNA fragments, that were then

184 end-repaired and ligated using paired-end sequencing adapters. The products were
185 then amplified to enrich for fragments carrying adapters ligated on both ends, thus
186 creating the final cDNA library. RNAseq was performed on the HiScan SQ platform
187 (Illumina) as 75 bp paired-end.

188 **RNAseq data analysis**

189 Raw paired-end reads obtained by the HiScan SQ were filtered and trimmed with the
190 tool AdapterRemoval (<http://code.google.com/p/adapterremoval/>) to exclude low
191 quality bases and sequence adapters. Short reads were mapped on human reference
192 genome hg19 (<https://genome.ucsc.edu/>) with the pipeline Bowtie/Tophat
193 (<http://ccb.jhu.edu/software/tophat/index.shtml>) and Samtools
194 (<http://samtools.sourceforge.net/>) was adopted to remove optical/PCR duplicates.
195 Gene expression quantification was performed with the Python package htseq-count
196 (<http://www-huber.embl.de/HTSeq/doc/overview.html>) using the Ensembl release 72
197 annotation features (<http://www.ensembl.org>). The raw counts were normalized with
198 the R-Bioconductor package edgeR (function calcNormFactors) as “count per million”
199 (cpm). A filter procedure was adopted to analyze only genes with cpm > 3 in at least
200 2/4 samples. This process allowed to include 9616 genes, that were analyzed with the
201 R-Bioconductor package limma to determine the differentially expressed genes. In
202 particular, the function lmFit was used to fit the linear model, and the function eBayes
203 was adopted to compute the moderate t-statistic. Genes were ranked in order of
204 evidence for differential expression using log2 fold change (log2FC) and *P* value.²¹
205 Multiple Experiment Viewer (MEV) (v4.8.1) was used to perform the analysis in two
206 different ways: unsupervised hierarchical clustering (distance: Manhattan; clustering
207 method: average) and principal component analysis. A total of 111 differentially
208 expressed genes were selected ($P \leq 10^{-3}$) for the evaluation of the functional

classification of biological processes and pathway over-representation, performed with the analytical tools PANTHER13.1 (Protein ANalysis THrough Evolutionary Relationships; <http://pantherdb.org>) and STRING. PANTHER is tightly integrated with a number of different genomic resources: the InterPro Consortium of protein classification resources, the Quest for Orthologs Consortium and the UniProt Reference Proteome data sets. PANTHER Over-representation tool includes functional annotations directly downloaded from the Gene Ontology (GO) Consortium, in addition to the phylogenetically inferred annotations.²² Analysis was performed using the option PANTHER Functional Classification and Over-representation Tests, using the PANTHER GO-Slim Biological process and the Fisher's Exact with false discovery rate (FDR) multiple test correction for statistical analysis. Independent analysis to observe protein-protein interaction was performed with STRING, a database of known and predicted protein-protein interactions. The interactions include direct (physical) and indirect (functional) associations; stemming from computational prediction, from knowledge transfer between organisms, and from interactions aggregated from other (primary) databases.^{23,24}

Quantitative real-time RT-qPCR

DNase I-treated RNA (200 ng) was used for reverse transcription (RT) with random hexamers using the Multiscribe RT system (ThermoFisher Scientific) at 48°C for 40 min in a final volume of 50 µl. *DNase I*-treated total RNA was obtained from a pool of commercially available fresh frozen tissue biopsies of five controls subjects (single vial purchased from AMSBIO, Abingdon, Oxford, UK; reference code: R1234106-P, lot number B209050, human normal adult esophageal total RNA); the other RNAs were obtained from fresh frozen tissue biopsies as described above.

RT-qPCR was performed with SYBRGreen, 0.5 μ M primers, in an ABI 7500 Real-Time PCR System (ThermoFisher Scientific). All target genes were normalized with the endogenous control (beta-actin) using the $\Delta\Delta$ Ct comparative method. Primers are available from the Authors on request.

Western blotting

Proteins were extracted from fresh frozen tissue biopsies of esophagus of achalasia patients and controls by sonication using the Diagenode Bioruptor Pico sonicator System (V 1.1) (10 cycles of 30 on/30 off; 20-60 kHz), in a volume of 50 μ l of Laemli buffer 1X. A pool of normal esophageal tissues was commercially available (Abcam, Cambridge, UK, reference code ab30243 - Human esophagus normal tissue lysate - total protein), the other tissues analyzed with western blotting were obtained from fresh frozen tissue biopsies of single cases and controls as reported in Supplementary Tables 1A and 1B. Proteins were visualized on Coomassie Blue gel for quality and quantity control. Western blot analysis was performed by SDS gel electrophoresis and transfer onto nitrocellulose membrane, using the TransBlot system (Bio-Rad Laboratories, Segrate, Italy). Primary antibodies used were the following: rabbit anti-INPP4B diluted 1:200 (Abcam); rabbit anti-c-KIT (Abcam) diluted 1:200; mouse anti-vinculin (Sigma-Aldrich, St. Louis, MO, USA) diluted at 1:5000; mouse anti-GAPDH 1:10000 (Abcam); anti p-Akt (Ser473), anti p-Akt (Thr308), anti Akt (Cell Signaling, Leiden, Netherlands), anti β -actin 1:10000 (Sigma-Aldrich). HRPO-conjugated secondary antibodies (Sigma-Aldrich) were diluted 1:35000 in blocking solution. Bands were visualized by the ECL method Supernova (Cyanagen, Bologna, Italy) using the Chemidoc XRS+ Imager and densitometric analysis was performed with Image lab Software (Bio-Rad Laboratories). All western blot analyses were

performed at least in duplicate for each protein extract from each patient and control tissue biopsy.

Immunohistochemistry

Immunohistochemistry was performed on paraffin-embedded adult human esophagus tissues according to protocols validated in our laboratory.²⁵ Immunohistochemistry analyses and image acquisitions were performed in our laboratory at the University of Bologna. Briefly, tissue sections were treated to remove paraffin embedding by sequential washes in xylene and graded ethanol. Antigen unmasking was performed by heating sections at 95°C in 10 mM Sodium citrate buffer, pH 6.0, for 10 min and subsequent cooling at room temperature for 30 min. To reduce endogenous peroxidases, tissue sections were treated with an ad hoc blocking kit (GeneTex Inc., Irvine, CA, USA) and incubated for 16 h at 4°C with the same primary antibodies used for western blotting, but diluted 1:50. 3,3'-diaminobenzidine staining was performed according to standard protocols (DAB500 IHC Select® kit, Merck Millipore, Darmstadt, Germany). Scores were assigned based on the intensity of DAB staining (0 = no staining; + = 10-50% staining; ++ = 50-90% staining; +++ = ≥90% staining of the areas; all images were acquired at 10x magnification) according to standard pathological assessment.²⁶ Three expert observers independently evaluated the images (E.B., F.B. and R. De G.), and their analyses were blinded regarding control vs. achalasia state. Image capturing of achalasia and control tissues was performed on a Nikon microscope using DS-5M digital camera (Nikon Instruments, Düsseldorf, Germany).

Statistical analysis

Quantitative difference in densitometry of western blots was performed with the Student's t-test option of GraphPad Quickstat calculator; statistical differences for the scores assigned to IHC samples from tissue biopsies was performed with Fisher's Test (4 x 2 contingency table) using the program Vassarstats.

Results

Whole transcriptome analysis via RNAseq

Total RNA extracted from esophageal biopsies of four cases (2F; age range: 30-58 yrs) and four controls (3F; age range: 27-50 yrs) was used for library preparation and sequencing on Illumina HiScan SQ platform. Raw data showing the total amount of reads/library and the mean coverage are reported in Supplementary Table 2, along with the mean coverage for each sample. Quantitative data analysis using Bioconductor from R package identified 111 genes with differential expression between cases and controls at a $P \leq 10^{-3}$ (Table 1). Compared to controls, 77 genes were downregulated and 34 genes were upregulated in the achalasia group. Hierarchical clustering considering the 111 genes was performed using MEV v4.8.1. As shown in the heat map in Figure 1A, a concordant signature of up- and down-regulation expression was evident between cases and controls. Analysis using PANTHER Functional classification test (PANTHER GO Slim Process) led us to functionally map a total of 109 out of the 111 differentially expressed genes to different biological processes, including, amongst others, cell adhesion, biogenesis, developmental, immune and metabolic processes and response to stimuli (<http://www.pantherdb.org/chart/pantherChart.jsp?listType=1&filterLevel=1&type=2&chartType=1&save=yes&basketItems=all&zoom=1.25&trackingId=4DCA8C9D00F5C4649E3257CE82CFAC3E>) (Figure 1B). PANTHER Over-representation Test

analysis was performed against the *H. sapiens* gene database, showing a set of over-represented biological processes in achalasia, including, amongst others, phosphorylation, the MAPK cascade signaling (including intracellular signal transduction and cell communication), regulation of phosphate metabolism and developmental processes, e.g. cell differentiation and death ($FDR < 0.05$; Table 2).

Network analysis was performed with STRING using the list of genes (the previously identified 111 genes) reported in Table 1, using the *H. sapiens* database as model organism, and the “whole genome” option as statistical background. A number of 104 out of 111 genes matched the STRING protein database and were included in the analysis (<https://string-db.org/cgi/network.pl?taskId=u9O5yLo4Lf2G>). Several pathways were identified that showed a functional enrichment for biological processes, such as regulation of development, cell differentiation, angiogenesis and vascular architecture, with significant *P* values reported in Table 3. Many protein-protein interactions converged on c-KIT (Figure 1C).

Among the dysregulated genes in achalasia, those differentially expressed with a significant $P \leq 10^{-4}$ were selected for further investigation, including *CYR61*, *CTGF*, *c-KIT*, *EGRI*, *LIF* and *CD69* (downregulated); and *AKAP6*, and *INPP4B* (overexpressed) (Table 1). To validate the data from whole transcriptome analysis, we performed quantitative real-time RT-qPCR using the total RNA of already sequenced samples (including two patients and one control). For each real-time RT-qPCR, raw data were normalized on a commercial pool of human normal esophagus RNA from fresh frozen tissue biopsies of five individuals (AMSBIO), using the $\Delta\Delta C_t$ method. Data reported in Figure 1D show independent technical replicates (same case-control samples, independent retro-transcription and real-time processes). A significant dysregulation of expression was confirmed for *c-KIT* and *INPP4B* (Figure 1D). These

findings prompted us to focus on these two molecular targets, i.e. *c-KIT* and *INPP4B*, which were down- and up-regulated, respectively.

Protein analysis of INPP4B and c-KIT confirmed the RNAseq data

The protein expression of c-KIT and INPP4B was studied by western blotting. In these experiments, control samples included a pool of normal esophageal tissues (Abcam) from five subjects in addition to control tissues obtained from single individual control subjects. Western blotting analysis for each tissue lysate was performed at least in two independent experiments, i.e. technical replicates. Equal amount of proteins was loaded for each sample and intensities were normalized using reference proteins. Representative examples of the protein patterns observed for c-KIT, INPP4B and reference proteins were reported in Figure 2A. Densitometric analysis of western blots was performed as indicated in Figure 2B. All cases and controls included in the western blotting analysis were reported in Supplementary Tables 1A and 1B. c-KIT downregulation was confirmed in tissue biopsies of achalasia patients compared to controls ($P= 0.0003$, Student's t-test; Figure 2B), whereas INPP4B overexpression was significantly detectable in achalasia patients vs. controls ($P=0.0381$; Student's t-test, Figure 2B).

Immunohistochemistry analysis was performed in order to confirm the western blot data and to determine the cellular localization of the proteins herein identified by western blot. The density of c-KIT immunoreactive cells (mainly with the typical shape of ICC) was lower in achalasia than in controls (Fisher's exact test, $P= 0.0005$, Figure 3A). Compared to controls, INPP4B immunoreactivity was more intense in achalasia patients. In INPP4B-positive cases, the immunoreactive signal was present in different cells including muscle cells and myenteric ganglia. INPP4B expression in

the normal tissues was very low or virtually absent (Fisher's exact test, $P=0.0023$; Figure 3B).

Phospho-Akt is down regulated in achalasia

As INPP4B is a negative regulator of Akt signaling, we investigated Akt phosphorylation status. Equal amount of proteins was loaded for each sample and intensities were normalized using reference proteins. Representative examples of the phosphorylation patterns observed for the two phosphorylation sites in Akt (Ser473, and Thr308) were reported in Figure 4A. Densitometric analysis, performed according to our previously published data,²⁷ revealed that tissue samples from achalasia patients presented a reduced Akt phosphorylation, in particular the phosphorylation at Ser473 was significantly decreased compared to control tissues ($P=0.0495$, Student's t-test; Figure 4B).

Discussion

Primary achalasia causes significant impairment of esophageal motility leading to symptom generation and overall reduced patients' quality of life. This esophageal dysmotility of the esophagus has a complex etio-pathogenesis. Recent findings indicate that both an inflammatory / immune-mediated insult, as exhibited by myenteric ganglionitis (likely driven by neurotropic, e.g. herpes, virus infection)²⁸ and circulating anti-neuronal antibodies, play a pathogenetic role. A genetic predisposition conferred by HLA genetic background²⁰ can contribute to neural abnormalities underlying achalasia. A predominant genetic component has been identified in well-defined conditions such as 'triple A' (also referred to Allgrove's syndrome), where mutations in the ALADIN gene¹⁴ were found in familial clusters. Other data derive

1
2
3 381 from *NOS1*, which encodes for the neuronal nitric oxide synthase. A stop codon
4
5 382 mutation of this gene has been reported in a family where two children manifested a
6
7 383 very severe clinical phenotype dominated by achalasia.¹³ Nevertheless, in the majority
8
9 384 of cases the factors causing achalasia remain to be elucidated. As a consequence, the
10
11 385 available therapeutic approaches are far from targeting the actual mechanisms leading
12
13 386 to the neural impairment recognized to be the *primum movens* of this severe
14
15 387 esophageal disorder. New understanding of achalasia, involving a deeper knowledge
16
17 388 of the attendant molecular mechanisms, should aim to a better patient management
18
19 389 and stop the disease at early stages. Therefore, the present study attempted to decipher
20
21 390 the altered molecular pathways in patients with achalasia. We strategically used
22
23 391 esophageal tissues from achalasic patients and examined gene expression via whole
24
25 392 transcriptome analysis in order to provide novel targets for a therapeutic approach.
26
27 393 From the RNAseq data we detected 111 genes with an altered expression. **Functional**
28
29 394 **classification and over-representation analysis of the biological processes, where**
30
31 395 **these genes mapped, was performed with two different bioinformatic tools,**
32
33 396 **PANTHER and STRING. Results showed a significant over-representation of**
34
35 397 **phosphorylation processes, intracellular signaling, cell communication and**
36
37 398 **development /differentiation processes, including cell death. These data suggest that**
38
39 399 **an imbalance of cell growth/survival vs. cell death** may cause the defects observed in
40
41 400 the achalasia tissues, not only in term of neuron loss, but also as an overall tissue
42
43 401 degeneration. **Notably, in a recent study, Palmieri et al. performed transcriptome**
44
45 402 **analysis on tissues of primary achalasia patients and identified a significant**
46
47 403 **enrichment of neuro-muscular and neuro-immune processes. These data support the**
48
49 404 **concept that achalasia results from degenerative alterations / loss of myenteric**
50
51
52
53
54
55
56
57
58
59
60

neurons mainly evoked by a chronic inflammatory infiltrate targeting the myenteric plexus.²⁹

Among the genes with significant dysregulation, we confirmed by real-time qPCR *c-KIT* downregulation and *INPP4B* upregulation, respectively. *c-KIT* significant downregulation, validated both via western blot and immunohistochemistry, confirms and expands previously reported data showing a loss of ICC network in tissues of patients with primary achalasia.⁹ Our data highlighting a significant decrease of c-KIT expression in human achalasia support the concept that stem cell factor, the major ligand to c-KIT, cannot mediate ICC maintenance and survival. Although we did not look into specific apoptotic mechanisms, it is likely that a programmed cell death can involve ICC in achalasia.³⁰ Since ICC play a role in esophageal motility, their depletion can contribute to the deranged mechanisms leading to altered motility in achalasia.³¹

The second gene for which we were able to confirm an altered expression at the protein level is INPP4B, encoding for inositol polyphosphate-4-phosphatase type II B, a negative regulator of Akt.^{32,33} The expression of this phosphatase was upregulated in many cell types in tissues from achalasic patients, indicating a general increase in inhibitory signals for cell survival, a mechanism stimulated by Akt-dependent pathways.³² Thus, an INPP4B increased expression can be correlated to the enrichment in genes involved in cell death. Notably, in achalasia tissues we observed a decrease in the phosphorylation of the Ser473 in Akt, which is a key phosphorylation step for its activation and function. Therefore, it may be postulated that in achalasia the altered molecular signaling led to an overall impaired cell survival, which, in the long term, generates a permanent tissue damage. Thus, one can assume that also ICCs, in addition to neurons, can be affected. Since many studies

430 have investigated the Akt / INPP4B pathway as a potential “druggable” route to block
431 tumor proliferation,^{33,34} the development of *ad hoc* molecules may become relevant
432 for patients with primary achalasia.

434 In conclusion, our study highlights the altered expression of two distinct genes, i.e. c-
435 KIT and INPP4B down- and up-regulation, in patients with primary achalasia. Our
436 results may provide a basis for future research aimed at investigating novel
437 therapeutic targets for patients with primary achalasia.

439 **Acknowledgements**

440 The authors wish to thank all patients that participated in the study. We thank Drs. A.
441 Gori, and V. Bertakis and Ms. G. Galiazzo for technical help.

444 **References**

- 445 1. Boeckxstaens GE, Zaninotto G, Richter JE. Achalasia. Lancet 2014;383:83-93.
446 2. Moonen A, Boeckxstaens G. Current diagnosis and management of achalasia. J
447 Clin Gastroenterology 2014;48:484-90.
448 3. Kahrilas PJ, Boeckxstaens G. The spectrum of achalasia: lessons from studies of
449 pathophysiology and high resolution manometry. Gastroenterology 2013;145:954-65.
450 4. Di Nardo G, Tullio-Pelet A, Annese V, et al. Idiopathic achalasia is not allelic to
451 alacrima achalasia adrenal insufficiency syndrome at the ALADIN locus. Dig Liver
452 Dis 2005;37:312-5.

- 453 5. Goldblum, JR, Rice, TW, Richter JE. Histopathologic features in
454 esophagomyotomy specimens from patients with achalasia. *Gastroenterology*
455 1996;111:648-54.
- 456 6. Roman S, Gyawali CP, Xiao Y, Pandolfino JE, Kahrilas PJ. The Chicago
457 classification of motility disorders: an update. *Gastrointest Endosc Clin North Am*
458 2014;24:545-61.
- 459 7. Boeckxstaens GE, Annese V, des Varannes SB, et al. European Achalasia Trial
460 Investigators. Pneumatic dilation versus laparoscopic Heller's myotomy for idiopathic
461 achalasia. *N Engl J Med* 2011;364:1807-16.
- 462 8. Ates F, Vaezi MF. The Pathogenesis and management of achalasia: Current status
463 and future directions. *Gut Liver* 2015;9:449-63.
- 464 9. Gockel I, Bohl JR, Eckardt VF, Junginger T. Reduction of interstitial cells of Cajal
465 (ICC) associated with neuronal nitric oxide synthase (n-NOS) in patients with
466 achalasia. *Am J Gastroenterol* 2008;103:856-64.
- 467 10. Saraiva MJM, Birken S, Costa PP, Goodman DS. Amyloid fibril protein in
468 familial amyloidotic polyneuropathy, Portuguese type: definition of molecular
469 abnormality in transthyretin (prealbumin). *J Clin Invest* 1984;74:104-19.
- 470 11. Sodikoff JB, Lo AA, Shetuni BB, Kahrilas PJ, Yang GY, Pandolfino JE.
471 Histopathologic patterns among achalasia subtypes. *Neurogastroenterol Motil*
472 2016;28:139-45.
- 473 12. Storch WB, Eckardt VF, Junginger T. Complement components and terminal
474 complement complex in oesophageal smooth muscle of patients with achalasia. *Cell*
475 *Mol Biol (Noisy-le-grand)* 2002;48:247-52.
- 476 13. Shteyer E, Edvardson S, Wynia-Smith SL, et al. Truncating mutation in the nitric
477 oxide synthase 1 gene is associated with infantile achalasia. *Gastroenterology*

2015;148:533-36.

14. Tullio-Pelet A, Salomon R, Hadj-Rabia S, et al. Mutant WD-repeat protein in triple-A syndrome. *Nat Genet* 2000;26:332-5.

15. Becker J, Haas SL, Mokrowiecka A, et al. The HLA-DQB1 insertion is a strong achalasia risk factor and displays a geospatial north-south gradient among Europeans. *Eur J Hum Genet* 2016;24:1228-31.

16. Verne GN, Sallustio JE, Eaker EY. Anti-myenteric neuronal antibodies in patients with achalasia. A prospective study. *Dig Dis Sci* 1997;42:307-13.

17. Ruiz-de-León A, Mendoza J, Sevilla-Mantilla C, et al. Myenteric antiplexus antibodies and class II HLA in achalasia. *Dig Dis Sci* 2002;47:15-19.

18. Latiano A, De Giorgio R, Volta U, et al. HLA and enteric antineuronal antibodies in patients with achalasia. *Neurogastroenterol Motil* 2006;18:520-25.

19. De la Concha EG, Fernandez-Arquero M, Mendoza JL, et al. Contribution of HLA class II genes to susceptibility in achalasia. *Tissue Antigens* 1998;52:381-84.

20. Gockel I, Becker J, Wouters MM, et al. Common variants in the HLA-DQ region confer susceptibility to idiopathic achalasia. *Nat Genet* 2014;46:901-4.

21. Nannini M, Astolfi A, Urbini M, et al. Integrated genomic study of quadruple-WT GIST (KIT/PDGFR/SDH/RAS pathway wild-type GIST). *BMC Cancer*. 2014;14:685.

22. Huang X, Muruganujan A, Tang H, et al. PANTHER version 11: expanded annotation data from Gene Ontology and Reactome pathways, and data analysis tool enhancements. *Nucleic Acids Research*, 2017;45:D183–9.

23. Szklarczyk D, Morris JH, Cook H, et al. The STRING database in 2017: quality-controlled protein-protein association networks, made broadly accessible. *Nucleic Acids Res*. 2017; 45: D362–D368.

24. Szklarczyk D, Franceschini A, Wyder S, et al. STRING v10: protein-protein interaction networks, integrated over the tree of life. *Nucleic Acids Res.* 2015 Jan; 43:D447-52.
25. Bonora E, Bianco F, Cordeddu L, et al. Mutations in RAD21 disrupt regulation of APOB in patients with chronic intestinal pseudo-obstruction. *Gastroenterology* 2015;148:771-82.e11.
26. Couch G, Redman JE, Wernisch L, Newton R, et al. The Discovery and Validation of Biomarkers for the Diagnosis of Esophageal Squamous Dysplasia and Squamous. *Cancer Prev Res (Phila).* 2016;9:558-66.
27. Buontempo F, Orsini E, Lonetti A, et al. Synergistic cytotoxic effects of bortezomib and CK2 inhibitor CX-4945 in acute lymphoblastic leukemia: turning off the prosurvival ER chaperone BIP/Grp78 and turning on the pro-apoptotic NF- κ B. *Oncotarget.* 2016;7:1323-40.
28. Moonen A, Boeckxstaens GE. Finding the right treatment for achalasia treatment: Risks, efficacy, complications. *Curr Treat Options Gastroenterol* 2016;14:420-28.
29. Palmieri O, Mazza T, Merla A, et al. Gene expression of muscular and neuronal pathways is cooperatively dysregulated in patients with idiopathic achalasia. *Sci Rep* 2016;6:31549.
30. Gibbons SJ, De Giorgio R, Faussone Pellegrini MS, et al. Apoptotic cell death of human interstitial cells of Cajal. *Neurogastroenterol Motil* 2009;21:85-93.
31. Farrugia G. Histologic changes in diabetic gastroparesis. *Gastroenterol Clin North Am.* 2015;44:31-8.
32. Rodgers SJ, Ferguson DT, Mitchell CA, Ooms LM. Regulation of PI3K effector signalling in cancer by the phosphoinositide phosphatases. *Biosci Rep* 2017;10:37(1).
33. Chew CL, Chen M, Pandolfi PP. Endosome and INPP4B. *Oncotarget* 2016;7:5-6.

1
2
3
4
5
6
7
8
9
10
11
12
13
14
15
16
17
18
19
20
21
22
23
24
25
26
27
28
29
30
31
32
33
34
35
36
37
38
39
40
41
42
43
44
45
46
47
48
49
50
51
52
53
54
55
56
57
58
59
60

528 34. Li Chew C, Lunardi A, Gulluni F, et al. In vivo role of INPP4B in tumor and
529 metastasis suppression through regulation of PI3K-AKT signaling at endosomes.
530 Cancer Discov 2015;5:740-51.
531

For Peer Review

Table 1. Genes differentially expressed in achalasia.

Genes overexpressed in achalasia are labeled in red. Green shadowed area indicates the genes with a $P \leq 10^{-4}$.

ENSEMBL transcript ID	GENE name	log2 Fold Change	P value
ENST00000451137	CYR61	-2.99	9.71E-06
ENST00000367976	CTGF	-2.74	1.19E-05
ENST00000513000	INPP4B	1.63	1.42E-04
ENST00000288135	KIT	-1.48	4.17E-04
ENST00000249075	LIF	-2.40	4.23E-04
ENST00000239938	EGR1	-1.95	4.65E-04
ENST00000228434	CD69	-3.84	4.94E-04
ENST00000280979	AKAP6	1.63	7.28E-04
ENST00000296464	HSPA4L	1.07	8.99E-04
ENST00000319653	FMN2	2.03	1.11E-03
ENST00000517956	FBXO32	1.26	1.12E-03
ENST00000265634	NPTX2	-1.88	1.20E-03
ENST00000550683	ACVRL1	-1.14	1.25E-03
ENST00000378827	BMP2	-1.99	1.51E-03
ENST00000371852	CH25H	-3.06	1.56E-03
ENST00000284669	KLHL41	2.43	1.58E-03
ENST00000436924	BRE	2.70	1.60E-03
ENST00000561981	FRRS1L	1.51	1.62E-03
ENST00000307792	SEMA3E	1.07	1.66E-03
ENST00000330871	SOCS3	-2.47	2.07E-03
ENST00000331569	ZNF703	1.18	2.30E-03
ENST00000305988	ADRB2	-1.41	2.47E-03
ENST00000420022	ADM5	-1.80	2.58E-03
ENST00000297316	SOX17	-1.82	2.76E-03
ENST00000252590	PLVAP	-1.29	2.77E-03
ENST00000256103	PMP2	-2.28	2.87E-03
ENST00000329099	FAM101B	-1.32	3.11E-03
ENST00000287814	TIMP4	-1.25	3.12E-03
ENST00000300177	GREM1	-2.58	3.29E-03
ENST00000485685	GGNBP2	-1.78	3.40E-03
ENST00000365328	RN7SK	-1.61	3.41E-03
ENST00000284878	CXADR	2.20	3.47E-03
ENST00000296046	CPA3	-1.76	3.52E-03
ENST00000302754	JUNB	-1.73	3.74E-03
ENST00000437551	PAX8-AS1	1.36	3.74E-03
ENST00000322507	COL12A1	-1.10	3.80E-03
ENST00000307637	C3AR1	-1.86	3.82E-03
ENST00000340695	SCXA	2.40	3.88E-03
ENST00000322954	UACA	0.94	3.89E-03

1
2
3
4
5
6
7
8
9
10
11
12
13
14
15
16
17
18
19
20
21
22
23
24
25
26
27
28
29
30
31
32
33
34
35
36
37
38
39
40
41
42
43
44
45
46
47
48
49
50
51
52
53
54
55
56
57
58
59
60

ENST00000055682	KIAA2022	1.00	3.92E-03
ENST00000379374	PHEX	-3.10	3.98E-03
ENST00000357949	SERTAD1	-1.45	4.02E-03
ENST00000230990	HBEGF	-2.36	4.08E-03
ENST00000359534	KCNK5	-2.25	4.16E-03
ENST00000224605	GDF10	-1.64	4.17E-03
ENST00000396184	PDE1C	1.02	4.32E-03
ENST00000373509	PIM1	-2.29	4.33E-03
ENST00000408965	CEBPD	-1.45	4.59E-03
ENST00000267984	MESDC1	-1.17	4.82E-03
ENST00000329608	CSF1	-1.16	4.92E-03
ENST00000344120	SPRY4	-1.18	5.13E-03
ENST00000395076	PPM1A	0.85	5.16E-03
ENST00000350896	MSR1	-1.37	5.21E-03
ENST00000366667	AGT	-1.68	5.22E-03
ENST00000263370	ITPKC	-1.75	5.24E-03
ENST00000259989	FGFBP2	-1.75	5.24E-03
ENST00000311922	TRIB1	-2.74	5.24E-03
ENST00000608521	MIR663A	2.80	5.25E-03
ENST00000377103	THBD	-2.31	5.27E-03
ENST00000422542	AC005682,5	-1.34	5.32E-03
ENST00000396037	ST8SIA1	1.75	5.39E-03
ENST00000264805	PDE5A	2.61	5.58E-03
ENST00000400546	NCAM2	-1.27	5.65E-03
ENST00000369026	MCL1	-1.16	6.00E-03
ENST00000515896	RNA5-8SP6	1.12	6.20E-03
ENST00000399799	ROCK1	0.96	6.23E-03
ENST00000273153	CSRNP1	-1.74	6.25E-03
ENST00000244221	PAIP2B	1.09	6.25E-03
ENST00000376414	GPR183	-1.77	6.40E-03
ENST00000500741	DYNLL1-AS1	1.16	6.57E-03
ENST00000308086	THAP2	0.91	6.67E-03
ENST00000274063	SFRP2	-1.92	6.68E-03
ENST00000290551	BTG2	-1.53	6.72E-03
ENST00000380392	C2CD4B	-2.57	6.78E-03
ENST00000410087	CERKL	-1.36	6.83E-03
ENST00000367558	RGS16	-2.28	7.09E-03
ENST00000256257	RNF122	-1.65	7.10E-03
ENST00000367511	FAM129A	0.64	7.12E-03
ENST00000592790	VMP1	-2.93	7.17E-03
ENST00000323040	GPR4	-1.97	7.27E-03
ENST00000307851	HAVCR2	-1.68	7.40E-03
ENST00000324559	ANO5	0.96	7.62E-03
ENST00000328041	SLC24A3	-1.35	7.63E-03
ENST00000311734	IL1RL1	-3.50	7.72E-03
ENST00000373313	MAFB	-1.65	8.05E-03

ENST00000382723	MSX1	-2.11	8.32E-03
ENST00000379731	B4GALT1	-1.49	8.33E-03
ENST00000329399	PDLIM1	-1.46	8.42E-03
ENST00000369583	DUSP5	-1.58	8.43E-03
ENST00000332029	SOCS1	-1.69	8.47E-03
ENST00000441535	FMO2	-1.27	8.55E-03
ENST00000256951	EMP1	-2.33	8.71E-03
ENST00000239223	DUSP1	-1.08	8.75E-03
ENST00000330106	CEND1	-2.85	8.84E-03
ENST00000498165	PPM1L	1.08	8.87E-03
ENST00000506002	MTND6P4	1.03	8.91E-03
ENST00000244050	SNAI1	-1.59	8.93E-03
ENST00000380874	FOXC1	-1.77	8.94E-03
ENST00000396073	ENAM	2.83	9.03E-03
ENST00000272928	ACKR3	-1.31	9.04E-03
ENST00000379359	RGCC	-1.11	9.22E-03
ENST00000333926	CISD1	0.80	9.30E-03
ENST00000367996	ADAMTS4	-4.18	9.37E-03
ENST00000380079	STEAP4	-2.07	9.38E-03
ENST00000413366	PRKCA	1.03	9.39E-03
ENST00000215794	USP18	-1.45	9.57E-03
ENST00000305352	S1PR1	-1.27	9.74E-03
ENST00000306065	ANKRD27	0.67	9.81E-03
ENST00000222390	HGF	-2.02	9.83E-03
ENST00000358432	EPHA2	-1.13	9.85E-03
ENST00000270001	ZFP14	0.88	9.89E-03

535

536

Table 2. Output of PANTHER Over-representation test of biological processes enriched for the genes differentially expressed in achalasia tissues, compared to H. sapiens gene PANTHER database.

PANTHER GO Slim Biological process	H. sapiens	Achalasia	Expected	Fold enrichment	Hierarchy (+/-)	raw P value	False Discovery Rate
Protein phosphorylation	81	4	.42	9.53	+	9.80e-04	3.99e-02
MAPK cascade	340	9	1.76	5.11	+	8.19e-05	6.66e-03
• intracellular signal transduction	1071	17	5.55	3.06	+	4.05e-05	4.94e-03
• signal transduction	2318	24	12.01	2.00	+	1.01e-03	3.54e-02
• Cell communication	2686	26	13.91	1.87	+	1.39e-03	3.76e-02
Regulation of catalytic activity	359	9	1.86	4.84	+	1.22e-04	7.47e-03
• regulation of molecular function	441	9	2.28	3.94	+	5.38e-04	2.62e-02
Regulation of phosphate metabolic process	537	12	2.78	4.31	+	2.64e-05	6.44e-03
Developmental process	1501	18	7.78	2.32	+	1.03e-03	3.13e-02

Only results with False Discovery Rate<0.05 are reported in the table.

Table 3: Output of STRING (protein-protein interaction and biological processes) for genes differentially regulated from whole transcriptome analysis of achalasia tissues.

	Pathway ID and description	Count in gene set	False Discovery Rate P values
Biological Process (GO)	GO 0051094 positive regulation of developmental process	29	1.97e-10
	GO 1901342 regulation of vascular development	15	8.62e-10
	GO 0045597 positive regulation of cell differentiation	24	1.44e-09
	GO 004565 regulation of angiogenesis	14	2.7e-09
	GO 2000026 regulation of multicellular organismal development	31	3.31e-09
Molecular function (GO)	GO 0001228 transcriptional activator activity, RNA polymerase II transcription regulatory region sequence-specific binding	9	0.0483
	GO 0005515 protein binding	40	0.0483
	GO 0008083 growth factor activity	3	0.0483
Cellular component (GO)	GO 005615 extracellular space	20	0.00342
	GO 0009986 cell surface	14	0.00552

Statistical background selected for the enrichment analysis set to “whole genome”.

Figure Legends

550

Figure 1. Differentially expressed genes in achalasia tissue. (A) Heat map showing the concordant differential expression observed in the tissues from achalasia patients compared to controls (for the genes reported in Table 1). Elaborated with MeV v4.8.1. (B) Biological processes of genes (GO-Slim Biological processes) differentially expressed in achalasia, as identified by PANTHER Functional Classification analysis. (C) Graphical output of significantly enriched protein-protein interactions determined with STRING analysis, showing the results of the 104 out of 111 dysregulated genes in achalasia, compared with data present in the STRING databases. The different colors in the figure inset identify the evidence for the different interactions (known; predicted; identified with other means, such as co-expression, data mining, and protein homology). The red square indicates c-KIT. (D) Real-time qRT-PCR data for *c-KIT* and *INPP4B*. Data from case and control tissue biopsies were normalized on a commercial pool of control tissue biopsies from esophagus. Student's t-test was performed and *P* values are indicated. Bars indicate standard deviations.

565

Figure 2. Western blot analysis of differentially expressed genes. (A) Example of the protein expression profiles in achalasia tissues compared to control samples for c-KIT and INPP4B. Western blotting was repeated in at least two independent experiments. (B) Densitometric analysis of the relative intensities for c-KIT and INPP4B. Quantitative data (mean values \pm standard deviation) from different experiments obtained from each individual were compared using Student's t-test for statistical analysis. For each sample, densitometric values were normalized on reference protein (vinculin). All experiments were carried out at least twice. Bars indicated standard deviations. *P* values are indicated in the graphs.

574

Figure 3. Immunostaining for c-KIT (A) and INPP4B (B). (A) Examples of the expression pattern for c-KIT in tissue biopsies from control (left) and achalasia patients (right). Arrows indicate the positive staining for c-KIT. c-KIT staining color histograms of controls (n=6) and cases (n=18) represent the number of samples assessed according to the semi-quantitative score. c-KIT immunolabeling differences in cases vs. controls were assessed by Fisher's exact test. (B) Examples of the expression pattern for INPP4B in tissue biopsies from control (left) and achalasia patients (right). INPP4B staining color histograms of controls (n=6) and cases (n=22) represent the number of samples assessed according to the semi-quantitative score. INPP4B immunolabeling differences in cases vs. controls were assessed by Fisher's exact test. Scale bars are 100µm as indicated.

Figure 4. Phospho-Akt is down regulated in achalasia. (A) Example of the protein expression profiles in achalasia tissues compared to control samples of phospho-Akt (Ser473; Thr308) and total Akt. (B) Quantitative data (mean values ± standard deviation) from different experiments (performed in duplicate) obtained from each individual were compared using Student's t-test. For each sample, densitometric values were normalized on reference protein (β-actin). The significantly different relative phospho-Akt (Ser473) levels comparing achalasia vs. control tissues, were reported in the histogram (P=0.0495, Student's t-test). Bars indicate standard deviations.

***INPP4B* overexpression and *c-KIT* downregulation in human achalasia**

Running title: INPP4B and c-KIT dysregulation in achalasia

Elena Bonora¹, Francesca Bianco^{1,2}, Agnese Stanzani^{1,2}, Fiorella Giancola^{1,2,3},
Annalisa Astolfi⁴, Valentina Indio⁴, Cecilia Evangelisti⁵, Alberto Maria Martelli⁵,
Elisa Boschetti^{1,3}, Marialuisa Lugaresi¹, Alexandros Ioannou¹, Francesco Torresan⁶,
Vincenzo Stanghellini¹, Paolo Clavenzani², Marco Seri¹, An Moonen⁷, Kim Van
Beek⁷, Mira Wouters⁷, Guy E. Boeckxstaens⁷, Giovanni Zaninotto⁸, Sandro Mattioli¹
and Roberto De Giorgio⁹

¹ Department of Medical and Surgical Sciences, DIMEC, University of Bologna and
St. Orsola-Malpighi Hospital, Bologna, Italy.

² Department of Medical and Veterinary Sciences, DIMEVET, University of Bologna,
Bologna, Italy.

³ Centro di Ricerca Biomedica Applicata, St.Orsola-Malpighi Hospital, Bologna, Italy

⁴ Interdepartmental Center for Cancer Research “G. Prodi” (CIRC), University of
Bologna, Bologna, Italy.

⁵ Department of Experimental Medicine, DIMES, University of Bologna, Bologna,
Italy.

⁶ Department of Digestive System, St. Orsola-Malpighi Hospital, Bologna, Italy.

⁷ Translational Research in GastroIntestinal Disorders (TARGID), Department of
Clinical and Experimental Medicine, KU Leuven University, Belgium.

⁸ Division of Surgery, Imperial College London, London, United Kingdom.

⁹ Department of Medical Sciences, Nuovo Arcispedale S. Anna at Cona (Ferrara),
University of Ferrara, Italy.

Funding

FB is recipient of a Telethon fellowship. This work was supported by grant
GGP15171 from Fondazione Telethon and University of Bologna (RFO funds) to EB
and RDeG. RDeG received research grants from Fondazione Del Monte of Bologna
and Ravenna. The funding bodies did not influence the content of this article.

Abbreviations

CPM - count per million, GO - gene ontology, LES - lower esophageal sphincter,
MEV - multiple experiment viewer, ICC - interstitial cells of Cajal, INPP4B - inositol
polyphosphate-4-phosphatase, type II B.

Correspondence address:

Roberto De Giorgio, MD, PhD, AGAF
Department of Medical Sciences,
University of Ferrara, Ferrara, Italy
e-mail: deg@aosp.bo.it
Tel.: +39-0532688156
Fax: +39-0532688156

Conflict of interest

The authors declare no conflict of interest

Author contribution

EB, RDeG conceived the study, performed data analysis and wrote the manuscript; AA, FB, VI, performed RNAseq and data analysis; AS, VB, FG, KVB, CE, EB performed immunostaining and western blotting analysis; ML, AI, FT, GZ; AM, MW, GEB, SM provided the clinical cases and tissue biopsies; SM, EB, RDeG, GEB, MS, VS performed critical revision of the manuscript. All authors read the final version of the paper.

Key points

- Primary achalasia is a disorder due to neuronal defects supplying the esophagus leading to altered peristalsis and lack of sphincter relaxation. Nonetheless, the molecular mechanisms involved in this condition are poorly understood.
- Transcriptomic analysis of achalasic tissues identified a dysregulated expression of different genes, in particular c-KIT (downregulated) and INPP4B (upregulated), the latter being linked to Akt pathway regulation.
- Our results unravel novel signaling pathways involved in the neuronal and interstitial cells of Cajal abnormalities in primary achalasia.

Abstract

Background & Aims: Achalasia is a rare motility disorder characterized by myenteric neuron and interstitial cells of Cajal (ICC) abnormalities leading to deranged/absent peristalsis and lack of relaxation of the lower esophageal sphincter. The mechanisms contributing to neuronal and ICC changes in achalasia are only partially understood. Our goal was to identify novel molecular features occurring in patients with primary achalasia.

Methods: Esophageal full-thickness biopsies from 42 (22 females; age range: 16-82 yrs) clinically, radiologically and manometrically characterized patients with primary achalasia were examined and compared to those obtained from ten subjects (controls) undergoing surgery for uncomplicated esophageal cancer (or upper stomach disorders). Tissue RNA extracted from biopsies of cases and controls was used for library preparation and sequencing. Data analysis was performed with the 'edgeR' option of R-Bioconductor. Data were validated by real-time RT-PCR, western blotting and immunohistochemistry.

Key Results: Quantitative transcriptome evaluation and cluster analysis revealed 111 differentially expressed genes, with a $P \leq 10^{-3}$. Nine genes with a $P \leq 10^{-4}$ were further validated. *CYR61*, *CTGF*, *c-KIT*, *DUSP5*, *EGR1* were downregulated, whereas *AKAP6* and *INPP4B* were upregulated in patients vs controls. Compared to controls, immunohistochemical analysis revealed a clear increase in INPP4B, whereas c-KIT immunolabeling resulted downregulated. Since INPP4B regulates Akt pathway, we used western blot to show that phospho-Akt was significantly reduced in achalasia patients vs controls.

1
2
3 103 **Conclusions & Inferences:** The identification of altered gene expression, including
4
5 104 *INPP4B*, a regulator of the Akt pathway, highlights novel signaling pathways
6
7 105 involved in the neuronal and ICC changes underlying primary achalasia.
8

9
10 106

11 107 **Key words:** Achalasia, cell signaling, c-KIT, INPP4B, transcriptome.
12
13
14 108

15
16
17
18
19
20
21
22
23
24
25
26
27
28
29
30
31
32
33
34
35
36
37
38
39
40
41
42
43
44
45
46
47
48
49
50
51
52
53
54
55
56
57
58
59
60

For Peer Review

Introduction

Achalasia is a primary motility disorder of the esophagus occurring at any age, with an estimated annual incidence of approximately 0.03-1 per 100 people and affecting both sexes equally.^{1,2} Achalasia can be classified into primary forms (mostly idiopathic), and cases associated with systemic disorders.^{3,4} From a pathogenetic stand-point, achalasia is characterized by a predominant loss of inhibitory myenteric neurons with a relative increase of cholinergic motoneurons⁵. Progressively degenerative processes may involve virtually all neurons over time. These neuronal changes result in an increase of the lower esophageal sphincter (LES) tone, which, in conjunction with an altered peristalsis of the esophageal body, represent the manometric correlate of any form of achalasia.⁶ Because of these functional abnormalities patients with achalasia complain of dysphagia, regurgitation and chest pain, often severe enough to require either surgery or pneumatic dilatation⁷. Mechanisms leading to esophageal myenteric neurodegeneration and loss include autoimmune responses likely triggered by environmental factors (e.g., neurotropic viruses) in genetically predisposed individuals.^{2,3,8} In addition to neurons, abnormalities of interstitial cells of Cajal (ICC), the pace-maker cells of the gastrointestinal tract, were demonstrated in patients with achalasia⁹.

The current standard for diagnosing achalasia is high-resolution manometry, although molecular biomarkers would be useful not only for diagnostic purposes, but also to address targeted therapeutic options so far not yet available. Proteomic analysis of sera from patients with achalasia and healthy individuals showed disease-related upregulation of transthyretin (TTR), a carrier of thyroid hormone thyroxine and a retinol-binding protein, associated with familial amyloid polyneuropathy.¹⁰ The

1
2
3 134 observed upregulation may correlate with the consequent neural degeneration
4
5 135 observed in achalasic patients.¹¹ Other studies demonstrated increased deposits of the
6
7 136 complement complex C5b-C9 and IgM within or proximal to ganglion cells of the
8
9 137 esophageal myenteric plexus.¹²
10
11 138 Achalasia due to rare genetic abnormalities includes recessive forms with mutations
12
13 139 in the neuronal nitric oxide synthase gene, *NOS1*¹³, or in *ALADIN* gene¹⁴ (Allgrove
14
15 140 syndrome or triple A syndrome, characterized by alacrima, achalasia and adrenal
16
17 141 cortex failure; OMIM #231550). Genome-wide and candidate gene association
18
19 142 studies have implicated the human leukocyte antigen (HLA) class II system as the
20
21 143 underlying genetic predisposing factor in achalasia. In particular, an 8-residues
22
23 144 insertion in the cytoplasmic tail of HLA-DQB1 has been identified as a strong risk
24
25 145 factor for achalasia, with a specific geospatial north-south gradient among
26
27 146 Europeans.¹⁵ Two amino acid substitutions in the extracellular domain of HLA-
28
29 147 DQ α 1, (lysine 41 encoded by HLA-DQA1*01:03) and of HLA-DQB1, (glutamic acid
30
31 148 45, encoded by HLA-DQB1*03:01 and HLA-DQB1*03:04) were characterized as
32
33 149 independent risk factors for achalasia and patients with the DQA1*0103 and
34
35 150 DQB1*0603 alleles have a significantly higher prevalence of anti-myenteric
36
37 151 antibodies.¹⁵⁻²⁰
38
39
40
41 152 Nevertheless, the mechanisms contributing to the observed neuronal and ICC changes
42
43 153 in achalasia are still partially understood. The aim of this study was to identify the
44
45 154 dysregulated molecular pathways / events occurring in primary (idiopathic) achalasia
46
47 155 to provide a molecular signature of primary achalasia.
48
49
50
51 156

52 157 **Materials and Methods**

53 158 **Patients and tissue biopsies**

A number of 42 (n= 20 from Italy; n= 22 from Belgium; 22 females; age range: 16-82 yrs) patients with a well-established clinical, radiological and manometric diagnosis of primary achalasia were recruited (Supplementary Table 1A). The included patients were all of Caucasian origin. Each patient underwent surgery and 1-2 tissue samples were obtained via a laparoscopic extramucosal Heller's myotomy extended 4-5 cm along the distal esophagus (i.e., 1-2 cm full-thickness biopsy containing the circular and longitudinal muscle with the associated enteric nervous system). Comparable control tissues were obtained from the corresponding esophageal region of 10 (3 females; age range: 45-87 yrs) controls, who were referred to surgery for uncomplicated esophageal cancer and upper stomach disorders, as reported in Supplementary Table 1B. Margins of all of sampled tissues were free of cancer. Signed informed consent was obtained for each subject enrolled in the study and data handling was performed according to the Helsinki declaration. The study was approved by the local Ethic Committee (study 42/2011/0/Oss protocol #877/211).

RNA extraction

Total RNA was extracted with the RiboPure kit from fresh frozen biopsies stored at -80°C in RNAlater, according to the manufacturer's instruction (Ambion, ThermoFisher Scientific, Waltham, MA, USA). RNA was resuspended in 40 µl of RNase-free water, and quality and quantity of RNA were evaluated on Agilent Bioanalyzer 2100 instrument (Agilent, Santa Clara, CA, USA). 150 ng of RNA was used for each library preparation, according to the TruSeq RNA Sample Prep v2 protocol (Illumina, San Diego, CA, USA). Poly(A)-RNA molecules from 500 ng of total RNA were purified using oligo-dT magnetic beads. Following purification, the mRNA was fragmented and randomly primed for reverse transcription followed by second-strand synthesis to create double-stranded cDNA fragments, that were then

184 end-repaired and ligated using paired-end sequencing adapters. The products were
185 then amplified to enrich for fragments carrying adapters ligated on both ends, thus
186 creating the final cDNA library. RNAseq was performed on the HiScan SQ platform
187 (Illumina) as 75 bp paired-end.

188 **RNAseq data analysis**

189 Raw paired-end reads obtained by the HiScan SQ were filtered and trimmed with the
190 tool AdapterRemoval (<http://code.google.com/p/adapterremoval/>) to exclude low
191 quality bases and sequence adapters. Short reads were mapped on human reference
192 genome hg19 (<https://genome.ucsc.edu/>) with the pipeline Bowtie/Tophat
193 (<http://ccb.jhu.edu/software/tophat/index.shtml>) and Samtools
194 (<http://samtools.sourceforge.net/>) was adopted to remove optical/PCR duplicates.
195 Gene expression quantification was performed with the Python package htseq-count
196 (<http://www-huber.embl.de/HTSeq/doc/overview.html>) using the Ensembl release 72
197 annotation features (<http://www.ensembl.org>). The raw counts were normalized with
198 the R-Bioconductor package edgeR (function calcNormFactors) as “count per million”
199 (cpm). A filter procedure was adopted to analyze only genes with cpm > 3 in at least
200 2/4 samples. This process allowed to include 9616 genes, that were analyzed with the
201 R-Bioconductor package limma to determine the differentially expressed genes. In
202 particular, the function lmFit was used to fit the linear model, and the function eBayes
203 was adopted to compute the moderate t-statistic. Genes were ranked in order of
204 evidence for differential expression using log₂ fold change (log₂FC) and *P* value.²¹
205 Multiple Experiment Viewer (MEV) (v4.8.1) was used to perform the analysis in two
206 different ways: unsupervised hierarchical clustering (distance: Manhattan; clustering
207 method: average) and principal component analysis. A total of 111 differentially
208 expressed genes were selected ($P \leq 10^{-3}$) for the evaluation of the functional

classification of biological processes and pathway over-representation, performed with the analytical tools PANTHER13.1 (Protein ANalysis THrough Evolutionary Relationships; <http://pantherdb.org>) and STRING. PANTHER is tightly integrated with a number of different genomic resources: the InterPro Consortium of protein classification resources, the Quest for Orthologs Consortium and the UniProt Reference Proteome data sets. PANTHER Over-representation tool includes functional annotations directly downloaded from the Gene Ontology (GO) Consortium, in addition to the phylogenetically inferred annotations.²² Analysis was performed using the option PANTHER Functional Classification and Over-representation Tests, using the PANTHER GO-Slim Biological process and the Fisher's Exact with false discovery rate (FDR) multiple test correction for statistical analysis. Independent analysis to observe protein-protein interaction was performed with STRING, a database of known and predicted protein-protein interactions. The interactions include direct (physical) and indirect (functional) associations; stemming from computational prediction, from knowledge transfer between organisms, and from interactions aggregated from other (primary) databases.^{23,24}

Quantitative real-time RT-qPCR

DNase I-treated RNA (200 ng) was used for reverse transcription (RT) with random hexamers using the Multiscribe RT system (ThermoFisher Scientific) at 48°C for 40 min in a final volume of 50 µl. *DNase I*-treated total RNA was obtained from a pool of commercially available fresh frozen tissue biopsies of five controls subjects (single vial purchased from AMSBIO, Abingdon, Oxford, UK; reference code: R1234106-P, lot number B209050, human normal adult esophageal total RNA); the other RNAs were obtained from fresh frozen tissue biopsies as described above.

RT-qPCR was performed with SYBRGreen, 0.5 μ M primers, in an ABI 7500 Real-Time PCR System (ThermoFisher Scientific). All target genes were normalized with the endogenous control (beta-actin) using the $\Delta\Delta$ Ct comparative method. Primers are available from the Authors on request.

Western blotting

Proteins were extracted from fresh frozen tissue biopsies of esophagus of achalasia patients and controls by sonication using the Diagenode Bioruptor Pico sonicator System (V 1.1) (10 cycles of 30 on/30 off; 20-60 kHz), in a volume of 50 μ l of Laemli buffer 1X. A pool of normal esophageal tissues was commercially available (Abcam, Cambridge, UK, reference code ab30243 - Human esophagus normal tissue lysate - total protein), the other tissues analyzed with western blotting were obtained from fresh frozen tissue biopsies of single cases and controls as reported in Supplementary Tables 1A and 1B. Proteins were visualized on Coomassie Blue gel for quality and quantity control. Western blot analysis was performed by SDS gel electrophoresis and transfer onto nitrocellulose membrane, using the TransBlot system (Bio-Rad Laboratories, Segrate, Italy). Primary antibodies used were the following: rabbit anti-INPP4B diluted 1:200 (Abcam); rabbit anti-c-KIT (Abcam) diluted 1:200; mouse anti-vinculin (Sigma-Aldrich, St. Louis, MO, USA) diluted at 1:5000; mouse anti-GAPDH 1:10000 (Abcam); anti p-Akt (Ser473), anti p-Akt (Thr308), anti Akt (Cell Signaling, Leiden, Netherlands), anti β -actin 1:10000 (Sigma-Aldrich). HRPO-conjugated secondary antibodies (Sigma-Aldrich) were diluted 1:35000 in blocking solution. Bands were visualized by the ECL method Supernova (Cyanagen, Bologna, Italy) using the Chemidoc XRS+ Imager and densitometric analysis was performed with Image lab Software (Bio-Rad Laboratories). All western blot analyses were

performed at least in duplicate for each protein extract from each patient and control tissue biopsy.

Immunohistochemistry

Immunohistochemistry was performed on paraffin-embedded adult human esophagus tissues according to protocols validated in our laboratory.²⁵ Immunohistochemistry analyses and image acquisitions were performed in our laboratory at the University of Bologna. Briefly, tissue sections were treated to remove paraffin embedding by sequential washes in xylene and graded ethanol. Antigen unmasking was performed by heating sections at 95°C in 10 mM Sodium citrate buffer, pH 6.0, for 10 min and subsequent cooling at room temperature for 30 min. To reduce endogenous peroxidases, tissue sections were treated with an ad hoc blocking kit (GeneTex Inc., Irvine, CA, USA) and incubated for 16 h at 4°C with the same primary antibodies used for western blotting, but diluted 1:50. 3,3'-diaminobenzidine staining was performed according to standard protocols (DAB500 IHC Select® kit, Merck Millipore, Darmstadt, Germany). Scores were assigned based on the intensity of DAB staining (0 = no staining; + = 10-50% staining; ++ = 50-90% staining; +++ = ≥90% staining of the areas; all images were acquired at 10x magnification) according to standard pathological assessment.²⁶ Three expert observers independently evaluated the images (E.B., F.B. and R. De G.), and their analyses were blinded regarding control vs. achalasia state. Image capturing of achalasia and control tissues was performed on a Nikon microscope using DS-5M digital camera (Nikon Instruments, Düsseldorf, Germany).

Statistical analysis

Quantitative difference in densitometry of western blots was performed with the Student's t-test option of GraphPad Quickstat calculator; statistical differences for the scores assigned to IHC samples from tissue biopsies was performed with Fisher's Test (4 x 2 contingency table) using the program Vassarstats.

Results

Whole transcriptome analysis via RNAseq

Total RNA extracted from esophageal biopsies of four cases (2F; age range: 30-58 yrs) and four controls (3F; age range: 27-50 yrs) was used for library preparation and sequencing on Illumina HiScan SQ platform. Raw data showing the total amount of reads/library and the mean coverage are reported in Supplementary Table 2, along with the mean coverage for each sample. Quantitative data analysis using Bioconductor from R package identified 111 genes with differential expression between cases and controls at a $P \leq 10^{-3}$ (Table 1). Compared to controls, 77 genes were downregulated and 34 genes were upregulated in the achalasia group. Hierarchical clustering considering the 111 genes was performed using MEV v4.8.1. As shown in the heat map in Figure 1A, a concordant signature of up- and down-regulation expression was evident between cases and controls. Analysis using PANTHER Functional classification test (PANTHER GO Slim Process) led us to functionally map a total of 109 out of the 111 differentially expressed genes to different biological processes, including, amongst others, cell adhesion, biogenesis, developmental, immune and metabolic processes and response to stimuli (<http://www.pantherdb.org/chart/pantherChart.jsp?listType=1&filterLevel=1&type=2&chartType=1&save=yes&basketItems=all&zoom=1.25&trackingId=4DCA8C9D00F5C4649E3257CE82CFAC3E>) (Figure 1B). PANTHER Over-representation Test

analysis was performed against the *H. sapiens* gene database, showing a set of over-represented biological processes in achalasia, including, amongst others, phosphorylation, the MAPK cascade signaling (including intracellular signal transduction and cell communication), regulation of phosphate metabolism and developmental processes, e.g. cell differentiation and death (FDR< 0.05; Table 2).

Network analysis was performed with STRING using the list of genes (the previously identified 111 genes) reported in Table 1, using the *H. sapiens* database as model organism, and the “whole genome” option as statistical background. A number of 104 out of 111 genes matched the STRING protein database and were included in the analysis (<https://string-db.org/cgi/network.pl?taskId=u9O5yLo4Lf2G>). Several pathways were identified that showed a functional enrichment for biological processes, such as regulation of development, cell differentiation, angiogenesis and vascular architecture, with significant *P* values reported in Table 3. Many protein-protein interactions converged on c-KIT (Figure 1C).

Among the dysregulated genes in achalasia, those differentially expressed with a significant $P \leq 10^{-4}$ were selected for further investigation, including *CYR61*, *CTGF*, *c-KIT*, *EGRI*, *LIF* and *CD69* (downregulated); and *AKAP6*, and *INPP4B* (overexpressed) (Table 1). To validate the data from whole transcriptome analysis, we performed quantitative real-time RT-qPCR using the total RNA of already sequenced samples (including two patients and one control). For each real-time RT-qPCR, raw data were normalized on a commercial pool of human normal esophagus RNA from fresh frozen tissue biopsies of five individuals (AMSBIO), using the $\Delta\Delta C_t$ method. Data reported in Figure 1D show independent technical replicates (same case-control samples, independent retro-transcription and real-time processes). A significant dysregulation of expression was confirmed for *c-KIT* and *INPP4B* (Figure 1D). These

findings prompted us to focus on these two molecular targets, i.e. *c-KIT* and *INPP4B*, which were down- and up-regulated, respectively.

Protein analysis of INPP4B and c-KIT confirmed the RNAseq data

The protein expression of c-KIT and INPP4B was studied by western blotting. In these experiments, control samples included a pool of normal esophageal tissues (Abcam) from five subjects in addition to control tissues obtained from single individual control subjects. Western blotting analysis for each tissue lysate was performed at least in two independent experiments, i.e. technical replicates. Equal amount of proteins was loaded for each sample and intensities were normalized using reference proteins. Representative examples of the protein patterns observed for c-KIT, INPP4B and reference proteins were reported in Figure 2A. Densitometric analysis of western blots was performed as indicated in Figure 2B. All cases and controls included in the western blotting analysis were reported in Supplementary Tables 1A and 1B. c-KIT downregulation was confirmed in tissue biopsies of achalasia patients compared to controls ($P=0.0003$, Student's t-test; Figure 2B), whereas INPP4B overexpression was significantly detectable in achalasia patients vs. controls ($P=0.0381$; Student's t-test, Figure 2B).

Immunohistochemistry analysis was performed in order to confirm the western blot data and to determine the cellular localization of the proteins herein identified by western blot. The density of c-KIT immunoreactive cells (mainly with the typical shape of ICC) was lower in achalasia than in controls (Fisher's exact test, $P=0.0005$, Figure 3A). Compared to controls, INPP4B immunoreactivity was more intense in achalasia patients. In INPP4B-positive cases, the immunoreactive signal was present in different cells including muscle cells and myenteric ganglia. INPP4B expression in

the normal tissues was very low or virtually absent (Fisher's exact test, $P= 0.0023$; Figure 3B).

Phospho-Akt is down regulated in achalasia

As INPP4B is a negative regulator of Akt signaling, we investigated Akt phosphorylation status. Equal amount of proteins was loaded for each sample and intensities were normalized using reference proteins. Representative examples of the phosphorylation patterns observed for the two phosphorylation sites in Akt (Ser473, and Thr308) were reported in Figure 4A. Densitometric analysis, performed according to our previously published data,²⁷ revealed that tissue samples from achalasia patients presented a reduced Akt phosphorylation, in particular the phosphorylation at Ser473 was significantly decreased compared to control tissues ($P=0.0495$, Student's t-test; Figure 4B).

Discussion

Primary achalasia causes significant impairment of esophageal motility leading to symptom generation and overall reduced patients' quality of life. This esophageal dysmotility of the esophagus has a complex etio-pathogenesis. Recent findings indicate that both an inflammatory / immune-mediated insult, as exhibited by myenteric ganglionitis (likely driven by neurotropic, e.g. herpes, virus infection)²⁸ and circulating anti-neuronal antibodies, play a pathogenetic role. A genetic predisposition conferred by HLA genetic background²⁰ can contribute to neural abnormalities underlying achalasia. A predominant genetic component has been identified in well-defined conditions such as 'triple A' (also referred to Allgrove's syndrome), where mutations in the ALADIN gene¹⁴ were found in familial clusters. Other data derive

1
2
3 381 from *NOS1*, which encodes for the neuronal nitric oxide synthase. A stop codon
4
5 382 mutation of this gene has been reported in a family where two children manifested a
6
7 383 very severe clinical phenotype dominated by achalasia.¹³ Nevertheless, in the majority
8
9 384 of cases the factors causing achalasia remain to be elucidated. As a consequence, the
10
11 385 available therapeutic approaches are far from targeting the actual mechanisms leading
12
13 386 to the neural impairment recognized to be the *primum movens* of this severe
14
15 387 esophageal disorder. New understanding of achalasia, involving a deeper knowledge
16
17 388 of the attendant molecular mechanisms, should aim to a better patient management
18
19 389 and stop the disease at early stages. Therefore, the present study attempted to decipher
20
21 390 the altered molecular pathways in patients with achalasia. We strategically used
22
23 391 esophageal tissues from achalasic patients and examined gene expression via whole
24
25 392 transcriptome analysis in order to provide novel targets for a therapeutic approach.
26
27 393 From the RNAseq data we detected 111 genes with an altered expression. Functional
28
29 394 classification and over-representation analysis of the biological processes, where
30
31 395 these genes mapped, was performed with two different bioinformatic tools,
32
33 396 PANTHER and STRING. Results showed a significant over-representation of
34
35 397 phosphorylation processes, intracellular signaling, cell communication and
36
37 398 development /differentiation processes, including cell death. These data suggest that
38
39 399 an imbalance of cell growth/survival vs. cell death may cause the defects observed in
40
41 400 the achalasia tissues, not only in term of neuron loss, but also as an overall tissue
42
43 401 degeneration. Notably, in a recent study, Palmieri et al. performed transcriptome
44
45 402 analysis on tissues of primary achalasia patients and identified a significant
46
47 403 enrichment of neuro-muscular and neuro-immune processes. These data support the
48
49 404 concept that achalasia results from degenerative alterations / loss of myenteric
50
51
52
53
54
55
56
57
58
59
60

neurons mainly evoked by a chronic inflammatory infiltrate targeting the myenteric plexus.²⁹

Among the genes with significant dysregulation, we confirmed by real-time qPCR *c-KIT* downregulation and *INPP4B* upregulation, respectively. *c-KIT* significant downregulation, validated both via western blot and immunohistochemistry, confirms and expands previously reported data showing a loss of ICC network in tissues of patients with primary achalasia.⁹ Our data highlighting a significant decrease of c-KIT expression in human achalasia support the concept that stem cell factor, the major ligand to c-KIT, cannot mediate ICC maintenance and survival. Although we did not look into specific apoptotic mechanisms, it is likely that a programmed cell death can involve ICC in achalasia.³⁰ Since ICC play a role in esophageal motility, their depletion can contribute to the deranged mechanisms leading to altered motility in achalasia.³¹

The second gene for which we were able to confirm an altered expression at the protein level is INPP4B, encoding for inositol polyphosphate-4-phosphatase type II B, a negative regulator of Akt.^{32,33} The expression of this phosphatase was upregulated in many cell types in tissues from achalasic patients, indicating a general increase in inhibitory signals for cell survival, a mechanism stimulated by Akt-dependent pathways.³² Thus, an INPP4B increased expression can be correlated to the enrichment in genes involved in cell death. Notably, in achalasia tissues we observed a decrease in the phosphorylation of the Ser473 in Akt, which is a key phosphorylation step for its activation and function. Therefore, it may be postulated that in achalasia the altered molecular signaling led to an overall impaired cell survival, which, in the long term, generates a permanent tissue damage. Thus, one can assume that also ICCs, in addition to neurons, can be affected. Since many studies

1
2
3 430 have investigated the Akt / INPP4B pathway as a potential “druggable” route to block
4
5 431 tumor proliferation,^{33,34} the development of *ad hoc* molecules may become relevant
6
7 432 for patients with primary achalasia.
8
9 433

10
11 434 In conclusion, our study highlights the altered expression of two distinct genes, i.e. c-
12
13 435 KIT and INPP4B down- and up-regulation, in patients with primary achalasia. Our
14
15 436 results may provide a basis for future research aimed at investigating novel
16
17 437 therapeutic targets for patients with primary achalasia.
18
19 438

20 438 21 22 439 **Acknowledgements**

23
24 440 The authors wish to thank all patients that participated in the study. We thank Drs. A.
25
26 441 Gori, and V. Bertakis and Ms. G. Galiazzo for technical help.
27
28 442

29 442 30 443 31 443 32 33 444 **References**

- 34
35 445 1. Boeckxstaens GE, Zaninotto G, Richter JE. Achalasia. Lancet 2014;383:83-93.
36
37 446 2. Moonen A, Boeckxstaens G. Current diagnosis and management of achalasia. J
38
39 447 Clin Gastroenterology 2014;48:484-90.
40
41 448 3. Kahrilas PJ, Boeckxstaens G. The spectrum of achalasia: lessons from studies of
42
43 449 pathophysiology and high resolution manometry. Gastroenterology 2013;145:954-65.
44
45 450 4. Di Nardo G, Tullio-Pelet A, Annese V, et al. Idiopathic achalasia is not allelic to
46
47 451 alacrima achalasia adrenal insufficiency syndrome at the ALADIN locus. Dig Liver
48
49 452 Dis 2005;37:312-5.
50
51
52
53
54
55
56
57
58
59
60

1
2
3 453 5. Goldblum, JR, Rice, TW, Richter JE. Histopathologic features in
4
5 454 esophagomyotomy specimens from patients with achalasia. *Gastroenterology*
6
7 455 1996;111:648-54.
8
9 456 6. Roman S, Gyawali CP, Xiao Y, Pandolfino JE, Kahrilas PJ. The Chicago
10
11 457 classification of motility disorders: an update. *Gastrointest Endosc Clin North Am*
12
13 458 2014;24:545-61.
14
15 459 7. Boeckxstaens GE, Annese V, des Varannes SB, et al. European Achalasia Trial
16
17 460 Investigators. Pneumatic dilation versus laparoscopic Heller's myotomy for idiopathic
18
19 461 achalasia. *N Engl J Med* 2011;364:1807-16.
20
21 462 8. Ates F, Vaezi MF. The Pathogenesis and management of achalasia: Current status
22
23 463 and future directions. *Gut Liver* 2015;9:449-63.
24
25 464 9. Gockel I, Bohl JR, Eckardt VF, Junginger T. Reduction of interstitial cells of Cajal
26
27 465 (ICC) associated with neuronal nitric oxide synthase (n-NOS) in patients with
28
29 466 achalasia. *Am J Gastroenterol* 2008;103:856-64.
30
31 467 10. Saraiva MJM, Birken S, Costa PP, Goodman DS. Amyloid fibril protein in
32
33 468 familial amyloidotic polyneuropathy, Portuguese type: definition of molecular
34
35 469 abnormality in transthyretin (prealbumin). *J Clin Invest* 1984;74:104-19.
36
37 470 11. Sodikoff JB, Lo AA, Shetuni BB, Kahrilas PJ, Yang GY, Pandolfino JE.
38
39 471 Histopathologic patterns among achalasia subtypes. *Neurogastroenterol Motil*
40
41 472 2016;28:139-45.
42
43 473 12. Storch WB, Eckardt VF, Junginger T. Complement components and terminal
44
45 474 complement complex in oesophageal smooth muscle of patients with achalasia. *Cell*
46
47 475 *Mol Biol (Noisy-le-grand)* 2002;48:247-52.
48
49 476 13. Shteyer E, Edvardson S, Wynia-Smith SL, et al. Truncating mutation in the nitric
50
51 477 oxide synthase 1 gene is associated with infantile achalasia. *Gastroenterology*
52
53
54
55
56
57
58
59
60

2015;148:533-36.

14. Tullio-Pelet A, Salomon R, Hadj-Rabia S, et al. Mutant WD-repeat protein in triple-A syndrome. *Nat Genet* 2000;26:332-5.

15. Becker J, Haas SL, Mokrowiecka A, et al. The HLA-DQB1 insertion is a strong achalasia risk factor and displays a geospatial north-south gradient among Europeans. *Eur J Hum Genet* 2016;24:1228-31.

16. Verne GN, Sallustio JE, Eaker EY. Anti-myenteric neuronal antibodies in patients with achalasia. A prospective study. *Dig Dis Sci* 1997;42:307-13.

17. Ruiz-de-León A, Mendoza J, Sevilla-Mantilla C, et al. Myenteric antiplexus antibodies and class II HLA in achalasia. *Dig Dis Sci* 2002;47:15-19.

18. Latiano A, De Giorgio R, Volta U, et al. HLA and enteric antineuronal antibodies in patients with achalasia. *Neurogastroenterol Motil* 2006;18:520-25.

19. De la Concha EG, Fernandez-Arquero M, Mendoza JL, et al. Contribution of HLA class II genes to susceptibility in achalasia. *Tissue Antigens* 1998;52:381-84.

20. Gockel I, Becker J, Wouters MM, et al. Common variants in the HLA-DQ region confer susceptibility to idiopathic achalasia. *Nat Genet* 2014;46:901-4.

21. Nannini M, Astolfi A, Urbini M, et al. Integrated genomic study of quadruple-WT GIST (KIT/PDGFR/SDH/RAS pathway wild-type GIST). *BMC Cancer*. 2014;14:685.

22. Huang X, Muruganujan A, Tang H, et al. PANTHER version 11: expanded annotation data from Gene Ontology and Reactome pathways, and data analysis tool enhancements. *Nucleic Acids Research*, 2017;45:D183–9.

23. Szklarczyk D, Morris JH, Cook H, et al. The STRING database in 2017: quality-controlled protein-protein association networks, made broadly accessible. *Nucleic Acids Res*. 2017; 45: D362–D368.

1
2
3 503 24. Szklarczyk D, Franceschini A, Wyder S, et al. STRING v10: protein-protein
4
5 504 interaction networks, integrated over the tree of life. *Nucleic Acids Res.* 2015 Jan;
6
7 505 43:D447-52.
8
9 506 25. Bonora E, Bianco F, Cordeddu L, et al. Mutations in RAD21 disrupt regulation of
10
11 507 APOB in patients with chronic intestinal pseudo-obstruction. *Gastroenterology*
12
13 508 2015;148:771-82.e11.
14
15 509 26. Couch G, Redman JE, Wernisch L, Newton R, et al. The Discovery and
16
17 510 Validation of Biomarkers for the Diagnosis of Esophageal Squamous Dysplasia and
18
19 511 Squamous. *Cancer Prev Res (Phila).* 2016;9:558-66.
20
21 512 27. Buontempo F, Orsini E, Lonetti A, et al. Synergistic cytotoxic effects of
22
23 513 bortezomib and CK2 inhibitor CX-4945 in acute lymphoblastic leukemia: turning off
24
25 514 the prosurvival ER chaperone BIP/Grp78 and turning on the pro-apoptotic NF- κ B.
26
27 515 *Oncotarget.* 2016;7:1323-40.
28
29 516 28. Moonen A, Boeckxstaens GE. Finding the right treatment for achalasia treatment:
30
31 517 Risks, efficacy, complications. *Curr Treat Options Gastroenterol* 2016;14:420-28.
32
33 518 29. Palmieri O, Mazza T, Merla A, et al. Gene expression of muscular and neuronal
34
35 519 pathways is cooperatively dysregulated in patients with idiopathic achalasia. *Sci Rep*
36
37 520 2016;6:31549.
38
39 521 30. Gibbons SJ, De Giorgio R, Faussone Pellegrini MS, et al. Apoptotic cell death of
40
41 522 human interstitial cells of Cajal. *Neurogastroenterol Motil* 2009;21:85-93.
42
43 523 31. Farrugia G. Histologic changes in diabetic gastroparesis. *Gastroenterol Clin North*
44
45 524 *Am.* 2015;44:31-8.
46
47 525 32. Rodgers SJ, Ferguson DT, Mitchell CA, Ooms LM. Regulation of PI3K effector
48
49 526 signalling in cancer by the phosphoinositide phosphatases. *Biosci Rep* 2017;10:37(1).
50
51 527 33. Chew CL, Chen M, Pandolfi PP. Endosome and INPP4B. *Oncotarget* 2016;7:5-6.
52
53
54
55
56
57
58
59
60

- 1
2
3 528 34. Li Chew C, Lunardi A, Gulluni F, et al. In vivo role of INPP4B in tumor and
4
5 529 metastasis suppression through regulation of PI3K-AKT signaling at endosomes.
6
7 530 Cancer Discov 2015;5:740-51.
8
9 531

For Peer Review

Table 1. Genes differentially expressed in achalasia.

Genes overexpressed in achalasia are labeled in red. Green shadowed area indicates the genes with a $P \leq 10^{-4}$.

ENSEMBL transcript ID	GENE name	log2 Fold Change	P value
ENST00000451137	CYR61	-2.99	9.71E-06
ENST00000367976	CTGF	-2.74	1.19E-05
ENST00000513000	INPP4B	1.63	1.42E-04
ENST00000288135	KIT	-1.48	4.17E-04
ENST00000249075	LIF	-2.40	4.23E-04
ENST00000239938	EGR1	-1.95	4.65E-04
ENST00000228434	CD69	-3.84	4.94E-04
ENST00000280979	AKAP6	1.63	7.28E-04
ENST00000296464	HSPA4L	1.07	8.99E-04
ENST00000319653	FMN2	2.03	1.11E-03
ENST00000517956	FBXO32	1.26	1.12E-03
ENST00000265634	NPTX2	-1.88	1.20E-03
ENST00000550683	ACVRL1	-1.14	1.25E-03
ENST00000378827	BMP2	-1.99	1.51E-03
ENST00000371852	CH25H	-3.06	1.56E-03
ENST00000284669	KLHL41	2.43	1.58E-03
ENST00000436924	BRE	2.70	1.60E-03
ENST00000561981	FRRS1L	1.51	1.62E-03
ENST00000307792	SEMA3E	1.07	1.66E-03
ENST00000330871	SOCS3	-2.47	2.07E-03
ENST00000331569	ZNF703	1.18	2.30E-03
ENST00000305988	ADRB2	-1.41	2.47E-03
ENST00000420022	ADM5	-1.80	2.58E-03
ENST00000297316	SOX17	-1.82	2.76E-03
ENST00000252590	PLVAP	-1.29	2.77E-03
ENST00000256103	PMP2	-2.28	2.87E-03
ENST00000329099	FAM101B	-1.32	3.11E-03
ENST00000287814	TIMP4	-1.25	3.12E-03
ENST00000300177	GREM1	-2.58	3.29E-03
ENST00000485685	GGNBP2	-1.78	3.40E-03
ENST00000365328	RN7SK	-1.61	3.41E-03
ENST00000284878	CXADR	2.20	3.47E-03
ENST00000296046	CPA3	-1.76	3.52E-03
ENST00000302754	JUNB	-1.73	3.74E-03
ENST00000437551	PAX8-AS1	1.36	3.74E-03
ENST00000322507	COL12A1	-1.10	3.80E-03
ENST00000307637	C3AR1	-1.86	3.82E-03
ENST00000340695	SCXA	2.40	3.88E-03
ENST00000322954	UACA	0.94	3.89E-03

ENST00000055682	KIAA2022	1.00	3.92E-03
ENST00000379374	PHEX	-3.10	3.98E-03
ENST00000357949	SERTAD1	-1.45	4.02E-03
ENST00000230990	HBEGF	-2.36	4.08E-03
ENST00000359534	KCNK5	-2.25	4.16E-03
ENST00000224605	GDF10	-1.64	4.17E-03
ENST00000396184	PDE1C	1.02	4.32E-03
ENST00000373509	PIM1	-2.29	4.33E-03
ENST00000408965	CEBPD	-1.45	4.59E-03
ENST00000267984	MESDC1	-1.17	4.82E-03
ENST00000329608	CSF1	-1.16	4.92E-03
ENST00000344120	SPRY4	-1.18	5.13E-03
ENST00000395076	PPM1A	0.85	5.16E-03
ENST00000350896	MSR1	-1.37	5.21E-03
ENST00000366667	AGT	-1.68	5.22E-03
ENST00000263370	ITPKC	-1.75	5.24E-03
ENST00000259989	FGFBP2	-1.75	5.24E-03
ENST00000311922	TRIB1	-2.74	5.24E-03
ENST00000608521	MIR663A	2.80	5.25E-03
ENST00000377103	THBD	-2.31	5.27E-03
ENST00000422542	AC005682,5	-1.34	5.32E-03
ENST00000396037	ST8SIA1	1.75	5.39E-03
ENST00000264805	PDE5A	2.61	5.58E-03
ENST00000400546	NCAM2	-1.27	5.65E-03
ENST00000369026	MCL1	-1.16	6.00E-03
ENST00000515896	RNA5-8SP6	1.12	6.20E-03
ENST00000399799	ROCK1	0.96	6.23E-03
ENST00000273153	CSRNP1	-1.74	6.25E-03
ENST00000244221	PAIP2B	1.09	6.25E-03
ENST00000376414	GPR183	-1.77	6.40E-03
ENST00000500741	DYNLL1-AS1	1.16	6.57E-03
ENST00000308086	THAP2	0.91	6.67E-03
ENST00000274063	SFRP2	-1.92	6.68E-03
ENST00000290551	BTG2	-1.53	6.72E-03
ENST00000380392	C2CD4B	-2.57	6.78E-03
ENST00000410087	CERKL	-1.36	6.83E-03
ENST00000367558	RGS16	-2.28	7.09E-03
ENST00000256257	RNF122	-1.65	7.10E-03
ENST00000367511	FAM129A	0.64	7.12E-03
ENST00000592790	VMP1	-2.93	7.17E-03
ENST00000323040	GPR4	-1.97	7.27E-03
ENST00000307851	HAVCR2	-1.68	7.40E-03
ENST00000324559	ANO5	0.96	7.62E-03
ENST00000328041	SLC24A3	-1.35	7.63E-03
ENST00000311734	IL1RL1	-3.50	7.72E-03
ENST00000373313	MAFB	-1.65	8.05E-03

1
2
3
4
5
6
7
8
9
10
11
12
13
14
15
16
17
18
19
20
21
22
23
24
25
26
27
28
29
30
31
32
33
34
35
36
37
38
39
40
41
42
43
44
45
46
47
48
49
50
51
52
53
54
55
56
57
58
59
60

ENST00000382723	MSX1	-2.11	8.32E-03
ENST00000379731	B4GALT1	-1.49	8.33E-03
ENST00000329399	PDLIM1	-1.46	8.42E-03
ENST00000369583	DUSP5	-1.58	8.43E-03
ENST00000332029	SOCS1	-1.69	8.47E-03
ENST00000441535	FMO2	-1.27	8.55E-03
ENST00000256951	EMP1	-2.33	8.71E-03
ENST00000239223	DUSP1	-1.08	8.75E-03
ENST00000330106	CEND1	-2.85	8.84E-03
ENST00000498165	PPM1L	1.08	8.87E-03
ENST00000506002	MTND6P4	1.03	8.91E-03
ENST00000244050	SNAI1	-1.59	8.93E-03
ENST00000380874	FOXC1	-1.77	8.94E-03
ENST00000396073	ENAM	2.83	9.03E-03
ENST00000272928	ACKR3	-1.31	9.04E-03
ENST00000379359	RGCC	-1.11	9.22E-03
ENST00000333926	CISD1	0.80	9.30E-03
ENST00000367996	ADAMTS4	-4.18	9.37E-03
ENST00000380079	STEAP4	-2.07	9.38E-03
ENST00000413366	PRKCA	1.03	9.39E-03
ENST00000215794	USP18	-1.45	9.57E-03
ENST00000305352	S1PR1	-1.27	9.74E-03
ENST00000306065	ANKRD27	0.67	9.81E-03
ENST00000222390	HGF	-2.02	9.83E-03
ENST00000358432	EPHA2	-1.13	9.85E-03
ENST00000270001	ZFP14	0.88	9.89E-03

535

536

Table 2. Output of PANTHER Over-representation test of biological processes enriched for the genes differentially expressed in achalasia tissues, compared to H. sapiens gene PANTHER database.

PANTHER GO Slim Biological process	<i>H. sapiens</i>	Achalasia	Expected	Fold enrichment	Hierarchy (+/-)	raw <i>P</i> value	False Discovery Rate
Protein phosphorylation	81	4	.42	9.53	+	9.80e-04	3.99e-02
MAPK cascade	340	9	1.76	5.11	+	8.19e-05	6.66e-03
• intracellular signal transduction	1071	17	5.55	3.06	+	4.05e-05	4.94e-03
• signal transduction	2318	24	12.01	2.00	+	1.01e-03	3.54e-02
• Cell communication	2686	26	13.91	1.87	+	1.39e-03	3.76e-02
Regulation of catalytic activity	359	9	1.86	4.84	+	1.22e-04	7.47e-03
• regulation of molecular function	441	9	2.28	3.94	+	5.38e-04	2.62e-02
Regulation of phosphate metabolic process	537	12	2.78	4.31	+	2.64e-05	6.44e-03
Developmental process	1501	18	7.78	2.32	+	1.03e-03	3.13e-02

Only results with False Discovery Rate<0.05 are reported in the table.

Table 3: Output of STRING (protein-protein interaction and biological processes) for genes differentially regulated from whole transcriptome analysis of achalasia tissues.

	Pathway ID and description	Count in gene set	False Discovery Rate <i>P</i> values
Biological Process (GO)	GO 0051094 positive regulation of developmental process	29	1.97e-10
	GO 1901342 regulation of vascular development	15	8.62e-10
	GO 0045597 positive regulation of cell differentiation	24	1.44e-09
	GO 004565 regulation of angiogenesis	14	2.7e-09
	GO 2000026 regulation of multicellular organismal development	31	3.31e-09
Molecular function (GO)	GO 0001228 transcriptional activator activity, RNA polymerase II transcription regulatory region sequence-specific binding	9	0.0483
	GO 0005515 protein binding	40	0.0483
	GO 0008083 growth factor activity	3	0.0483
Cellular component (GO)	GO 005615 extracellular space	20	0.00342
	GO 0009986 cell surface	14	0.00552

Statistical background selected for the enrichment analysis set to “whole genome”.

Figure Legends

Figure 1. Differentially expressed genes in achalasia tissue. (A) Heat map showing the concordant differential expression observed in the tissues from achalasia patients compared to controls (for the genes reported in Table 1). Elaborated with MeV v4.8.1. (B) Biological processes of genes (GO-Slim Biological processes) differentially expressed in achalasia, as identified by PANTHER Functional Classification analysis. (C) Graphical output of significantly enriched protein-protein interactions determined with STRING analysis, showing the results of the 104 out of 111 dysregulated genes in achalasia, compared with data present in the STRING databases. The different colors in the figure inset identify the evidence for the different interactions (known; predicted; identified with other means, such as co-expression, data mining, and protein homology). The red square indicates c-KIT. (D) Real-time qRT-PCR data for *c-KIT* and *INPP4B*. Data from case and control tissue biopsies were normalized on a commercial pool of control tissue biopsies from esophagus. Student's t-test was performed and *P* values are indicated. Bars indicate standard deviations.

Figure 2. Western blot analysis of differentially expressed genes. (A) Example of the protein expression profiles in achalasia tissues compared to control samples for c-KIT and INPP4B. Western blotting was repeated in at least two independent experiments. (B) Densitometric analysis of the relative intensities for c-KIT and INPP4B. Quantitative data (mean values \pm standard deviation) from different experiments obtained from each individual were compared using Student's t-test for statistical analysis. For each sample, densitometric values were normalized on reference protein (vinculin). All experiments were carried out at least twice. Bars indicated standard deviations. *P* values are indicated in the graphs.

575

Figure 3. Immunostaining for c-KIT (A) and INPP4B (B). (A) Examples of the expression pattern for c-KIT in tissue biopsies from control (left) and achalasia patients (right). Arrows indicate the positive staining for c-KIT. c-KIT staining color histograms of controls (n=6) and cases (n=18) represent the number of samples assessed according to the semi-quantitative score. c-KIT immunolabeling differences in cases vs. controls were assessed by Fisher's exact test. (B) Examples of the expression pattern for INPP4B in tissue biopsies from control (left) and achalasia patients (right). INPP4B staining color histograms of controls (n=6) and cases (n=22) represent the number of samples assessed according to the semi-quantitative score. INPP4B immunolabeling differences in cases vs. controls were assessed by Fisher's exact test. Scale bars are 100µm as indicated.

587

Figure 4. Phospho-Akt is down regulated in achalasia. (A) Example of the protein expression profiles in achalasia tissues compared to control samples of phospho-Akt (Ser473; Thr308) and total Akt. (B) Quantitative data (mean values \pm standard deviation) from different experiments (performed in duplicate) obtained from each individual were compared using Student's t-test. For each sample, densitometric values were normalized on reference protein (β -actin). The significantly different relative phospho-Akt (Ser473) levels comparing achalasia vs. control tissues, were reported in the histogram (P=0.0495, Student's t-test). Bars indicate standard deviations.

597

1
2
3
4
5
6
7
8
9
10
11
12
13
14
15
16
17
18
19
20
21
22
23
24
25
26
27
28
29
30
31
32
33
34
35
36
37
38
39
40
41
42
43
44
45
46
47
48
49
50
51
52
53
54
55
56
57
58
59
60

Supplementary Table 1: Clinical and epidemiological data of achalasia patients (a) and controls (b)

a) Achalasia

ACHA pts ID	Sex	Age	Age at diagnosis	LES basal pressure (mm Hg)	Duration of symptoms before diagnosis(yrs)	Type of molecular analysis
ITA_ACHA77	M	43	30	15	15	wb
ITA_ACHA69	M	84	83	53	20	wb
ITA_ACHA74	M	42	41	22.5	5	wb
ITA_ACHA59	F	51	50	20	3	wb/IHC
ITA_ACHA81	F	24	20	18	5	wb
ITA_ACHA40	F	42	39	28	8	wb
ITA_ACHA17	F	46	45	20	10	wb
ITA_ACHA76	M	55	54	24	10	wb
ITA_ACHA71	F	72	70	15	8	wb
ITA_ACHA34	M	68	67	44	8	RNAseq
ITA_ACHA16	F	25	24	18	2	RNAseq
ITA_ACHA75	F	75	58	15	25	IHC
ITA_ACHA37	F	64	61	18	4	RNAseq/RT-qPCR/wb/IHC
ITA_ACHA34	M	58	57	35	20	/wb
ITA_ACHA02	F	37	34	25	4	wb/IHC
ITA_ACHA73	M	81	78	28	4	wb
ITA_ACHA33	M	68	67	44	2	RNAseq/RT-qPCR/wb/IHC
ITA_ACHA25	M	66	64	22	3	wb
ITA_ACHA78	F	36	36	15	1	IHC
ITA_ACHA66	F	41	40	23	20	wb
BE_ACHA5051	F	16	16	37	6	IHC
BE_ACHA5208	M	69	69	na ^{a)}	7	IHC
BE_ACHA5691	F	82	82	na	2.5	IHC
BE_ACHA6936	F	20	20	38	2	IHC
BE_ACHA7521	F	63	63	35.3	0.42	IHC
BE_ACHA5466	M	22	22	27.5	1	IHC
BE_ACHA5768	M	44	44	33	1.5	IHC
BE_ACHA6790	F	69	69	35.6	2	IHC
BE_ACHA810	M	61	61	30	15	IHC
BE_ACHA8705	M	65	65	na	10	IHC
BE_ACHA1059	M	28	28	na ^{a)}	7	IHC
BE_ACHA8154	F	42	42	68	0.58	IHC
BE_ACHA302	M	50	50	51	3	IHC
BE_ACHA479	M	50	50	34	3	IHC
BE_ACHA7818	F	33	33	38	0.17	IHC
BE_ACHA8199	M	24	24	103	6	IHC
BE_ACHA8347	F	21	21	na ^{b)}	4	IHC

BE_ACHA5260	F	32	32	48.3	2	IHC
BE_ACHA5295	F	35	35	na	6	IHC
BE_ACHA1730	M	57	57	nm	5	IHC
BE_ACHA3017	M	49	49	42.3	2	IHC
BE_ACHA3354	F	49	49	80.3	8	IHC

Legends: na= not available; nm= not measurable; ^{a)} type I; ^{b)} type II; wb= western blotting; IHC= immunohistochemistry.

b) controls

ID patients	Age	Sex	Pathology	Surgery	Histology	Type of molecular analysis
ITA_CNT_01	64	F	Gastroesophageal reflux	Antireflux Nissen fundoplication	-	IHC
ITA_CNT_02	45	M	Gastroesophageal reflux	Antireflux Nissen fundoplication	-	IHC
ITA_CNT_03	77	M	Esophageal adenocarcinoma - Siewert II	Total gastrectomy and resection of the distal esophagus (10 cm section above the diaphragmatic hiatus)	Intestinal adenocarcinoma (T3-N1-M0). Tumor-free margins	wb/IHC
ITA_CNT_70	55	M	Megaesophagus	Partial esophagectomy with gastro-esophageal reconstruction		IHC
ITA_CNT_72	87	M	Esophageal adenocarcinoma - Siewert I	Partial esophagectomy with gastro-esophageal reconstruction	Intestinal adenocarcinoma (T2-N1-M0). Tumor-free margins	IHC
ITA_CNT_04	69	M	Esophageal adenocarcinoma - Siewert II	Total gastrectomy and resection of the distal esophagus (10 cm section above the diaphragmatic hiatus)	Intestinal adenocarcinoma (T4-N3-M0). Tumor-free margins	IHC
ITA_CNT_26	49	F	Gastroesophageal reflux	Antireflux Nissen fundoplication	-	RNAseq/wb
ITA_CNT_23	46	F	Gastroesophageal reflux	Antireflux Nissen fundoplication	-	RNAseq/wb/IHC
ITA_CNT_41	66	M	Esophageal adenocarcinoma - Siewert I	Partial esophagectomy with gastro-esophageal reconstruction	Intestinal adenocarcinoma (T2-N1-M0). Tumor-free margins	RNAseq/wb
ITA_CNT_52	57	M	Esophageal adenocarcinoma - Siewert I	Partial esophagectomy with gastro-esophageal reconstruction	Intestinal adenocarcinoma (T3-N3-M0). Tumor-free margins	RNAseq/RT-qPCR/wb/IHC

1
2
3
4
5
6
7
8
9
10
11
12
13
14
15
16
17
18
19
20
21
22
23
24
25
26
27
28
29
30
31
32
33
34
35
36
37
38
39
40
41
42
43
44
45
46
47
48
49
50
51
52
53
54
55
56
57
58
59
60

Supplementary Table S2. Total read number and mean coverage of RNAseq libraries.

Sample ID	Total read number	Mean coverage (X)
ITA_ACHA16	96,763,286	63
ITA_ACHA34	79,986,036	43
ITA_ACHA37	85,671,948	47
ITA_ACHA33	74,486,236	55
ITA_CNT29	70,830,832	36
ITA_CNT26	70,217,988	55
ITA_CNT41	83,327,050	64
ITA_CNT52	81,841,600	68

Supplementary Table 1: Clinical and epidemiological data of achalasia patients (a) and controls (b)**a) Achalasia**

ACHA pts ID	Sex	Age	Age at diagnosis	LES basal pressure (mm Hg)	Duration of symptoms before diagnosis(yrs)	Type of molecular analysis
ITA_ACHA77	M	43	30	15	15	wb
ITA_ACHA69	M	84	83	53	20	wb
ITA_ACHA74	M	42	41	22.5	5	wb
ITA_ACHA59	F	51	50	20	3	wb/IHC
ITA_ACHA81	F	24	20	18	5	wb
ITA_ACHA40	F	42	39	28	8	wb
ITA_ACHA17	F	46	45	20	10	wb
ITA_ACHA76	M	55	54	24	10	wb
ITA_ACHA71	F	72	70	15	8	wb
ITA_ACHA34	M	68	67	44	8	RNAseq
ITA_ACHA16	F	25	24	18	2	RNAseq
ITA_ACHA75	F	75	58	15	25	IHC
ITA_ACHA37	F	64	61	18	4	RNAseq/RT-qPCR/wb/IHC
ITA_ACHA34	M	58	57	35	20	/wb
ITA_ACHA02	F	37	34	25	4	wb/IHC
ITA_ACHA73	M	81	78	28	4	wb
ITA_ACHA33	M	68	67	44	2	RNAseq/RT-qPCR/wb/IHC
ITA_ACHA25	M	66	64	22	3	wb
ITA_ACHA78	F	36	36	15	1	IHC
ITA_ACHA66	F	41	40	23	20	wb
BE_ACHA5051	F	16	16	37	6	IHC
BE_ACHA5208	M	69	69	na ^{a)}	7	IHC
BE_ACHA5691	F	82	82	na	2.5	IHC
BE_ACHA6936	F	20	20	38	2	IHC
BE_ACHA7521	F	63	63	35.3	0.42	IHC
BE_ACHA5466	M	22	22	27.5	1	IHC
BE_ACHA5768	M	44	44	33	1.5	IHC
BE_ACHA6790	F	69	69	35.6	2	IHC
BE_ACHA810	M	61	61	30	15	IHC
BE_ACHA8705	M	65	65	na	10	IHC
BE_ACHA1059	M	28	28	na ^{a)}	7	IHC
BE_ACHA8154	F	42	42	68	0.58	IHC
BE_ACHA302	M	50	50	51	3	IHC
BE_ACHA479	M	50	50	34	3	IHC
BE_ACHA7818	F	33	33	38	0.17	IHC
BE_ACHA8199	M	24	24	103	6	IHC
BE_ACHA8347	F	21	21	na ^{b)}	4	IHC

BE_ACHA5260	F	32	32	48.3	2	IHC
BE_ACHA5295	F	35	35	na	6	IHC
BE_ACHA1730	M	57	57	nm	5	IHC
BE_ACHA3017	M	49	49	42.3	2	IHC
BE_ACHA3354	F	49	49	80.3	8	IHC

Legends: na= not available; nm= not measurable; ^{a)} type I; ^{b)} type II; wb= western blotting; IHC= immunohistochemistry.

b) controls

ID patients	Age	Sex	Pathology	Surgery	Histology	Type of molecular analysis
ITA_CNT_01	64	F	Gastroesophageal reflux	Antireflux Nissen fundoplication	-	IHC
ITA_CNT_02	45	M	Gastroesophageal reflux	Antireflux Nissen fundoplication	-	IHC
ITA_CNT_03	77	M	Esophageal adenocarcinoma - Siewert II	Total gastrectomy and resection of the distal esophagus (10 cm section above the diaphragmatic hiatus)	Intestinal adenocarcinoma (T3-N1-M0). Tumor-free margins	wb/IHC
ITA_CNT_70	55	M	Megaesophagus	Partial esophagectomy with gastro-esophageal reconstruction		IHC
ITA_CNT_72	87	M	Esophageal adenocarcinoma - Siewert I	Partial esophagectomy with gastro-esophageal reconstruction	Intestinal adenocarcinoma (T2-N1-M0). Tumor-free margins	IHC
ITA_CNT_04	69	M	Esophageal adenocarcinoma - Siewert II	Total gastrectomy and resection of the distal esophagus (10 cm section above the diaphragmatic hiatus)	Intestinal adenocarcinoma (T4-N3-M0). Tumor-free margins	IHC
ITA_CNT_26	49	F	Gastroesophageal reflux	Antireflux Nissen fundoplication	-	RNAseq/wb
ITA_CNT_23	46	F	Gastroesophageal reflux	Antireflux Nissen fundoplication	-	RNAseq/wb/IHC
ITA_CNT_41	66	M	Esophageal adenocarcinoma - Siewert I	Partial esophagectomy with gastro-esophageal reconstruction	Intestinal adenocarcinoma (T2-N1-M0). Tumor-free margins	RNAseq/wb
ITA_CNT_52	57	M	Esophageal adenocarcinoma - Siewert I	Partial esophagectomy with gastro-esophageal reconstruction	Intestinal adenocarcinoma (T3-N3-M0). Tumor-free margins	RNAseq/RT-qPCR/wb/IHC

Supplementary Table S2. Total read number and mean coverage of RNAseq libraries.

Sample ID	Total read number	Mean coverage (X)
ITA_ACHA16	96,763,286	63
ITA_ACHA34	79,986,036	43
ITA_ACHA37	85,671,948	47
ITA_ACHA33	74,486,236	55
ITA_CNT29	70,830,832	36
ITA_CNT26	70,217,988	55
ITA_CNT41	83,327,050	64
ITA_CNT52	81,841,600	68

1
2
3
4
5 Supporting Material for reviewers Only
6
7
8
9

New! PANTHER13.1 released.

Analysis Summary: Please report in publication ?

Analysis Type: PANTHER Overrepresentation Test (Released 20171205)

Annotation Version and Release Date: PANTHER version 13.1 Released 2018-02-03

Analyzed List: Client Text Box Input (Homo sapiens) Change

Reference List: Homo sapiens (all genes in database) Change

Annotation Data Set: PANTHER GO-Slim Biological Process ▼

Test Type: ☒ Fisher's Exact with FDR multiple test correction ☐ Binomial

Results ?

	Reference list	Client Text Box Input
Mapped IDs:	21042 out of 21042	105 out of 109
Unmapped IDs:	0	7
Multiple mapping information:	0	4

Export results View: -- Please select a chart to display -- ▼

Displaying only results with False Discovery Rate < 0.05; [click here to display all results](#)

	Homo sapiens (REF)	Client Text Box Input (▼ Hierarchy NEW! ?)					
	#	#	expected	Fold Enrichment	+/-	raw P value	FDR
PANTHER GO-Slim Biological Process							
protein phosphorylation	81	4	.42	9.53	+	9.80E-04	3.99E-02
MAPK cascade	340	9	1.76	5.11	+	8.19E-05	6.66E-03
intracellular signal transduction	1071	17	5.55	3.06	+	4.05E-05	4.94E-03
signal transduction	2318	24	12.01	2.00	+	1.01E-03	3.54E-02
cell communication	2686	26	13.91	1.87	+	1.39E-03	3.76E-02
regulation of catalytic activity	359	9	1.86	4.84	+	1.22E-04	7.47E-03
regulation of molecular function	441	9	2.28	3.94	+	5.38E-04	2.62E-02
regulation of phosphate metabolic process	537	12	2.78	4.31	+	2.64E-05	6.44E-03
developmental process	1501	18	7.78	2.32	+	1.03E-03	3.13E-02

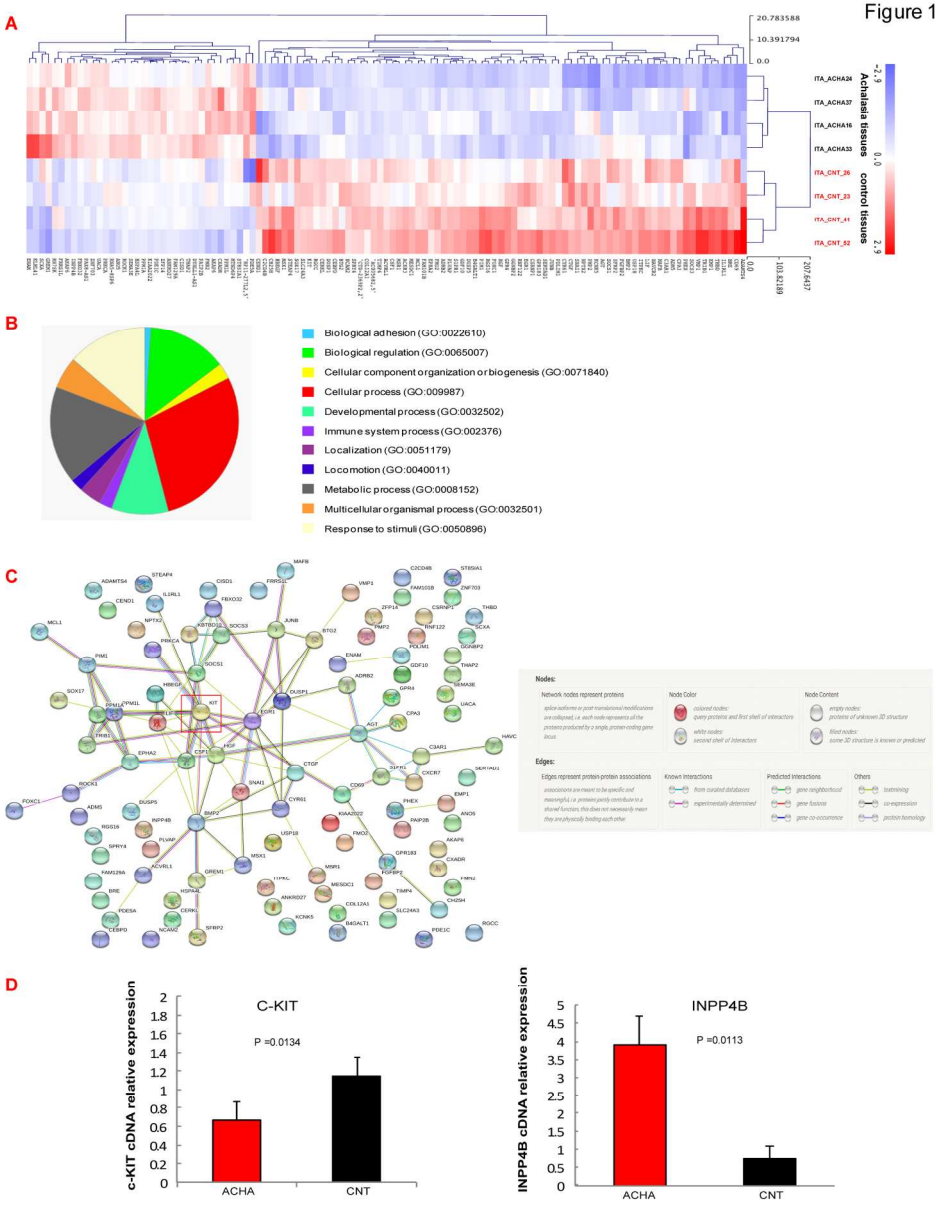


Figure 1. Differentially expressed genes in achalasia tissue. (A) Heat map showing the concordant differential expression observed in the tissues from achalasia patients compared to controls (for the genes reported in Table 1). Elaborated with MeV v4.8.1. (B) Biological processes of genes (GO-Slim Biological processes) differentially expressed in achalasia, as identified by PANTHER Functional Classification analysis. (C) Graphical output of significantly enriched protein-protein interactions determined with STRING analysis, showing the results of the 104 out of 111 dysregulated genes in achalasia, compared with data present in the STRING databases. The different colors in the figure inset identify the evidence for the different interactions (known; predicted; identified with other means, such as co-expression, data mining, and protein homology). The red square indicates c-KIT. (D) Real-time qRT-PCR data for c-KIT and INPP4B. Data from case and control tissue biopsies were normalized on a commercial pool of control tissue biopsies from esophagus. Student's t-test was performed and P values are indicated. Bars indicate standard deviations.

164x209mm (300 x 300 DPI)

1
2
3
4
5
6
7
8
9
10
11
12
13
14
15
16
17
18
19
20
21
22
23
24
25
26
27
28
29
30
31
32
33
34
35
36
37
38
39
40
41
42
43
44
45
46
47
48
49
50
51
52
53
54
55
56
57
58
59
60

For Peer Review

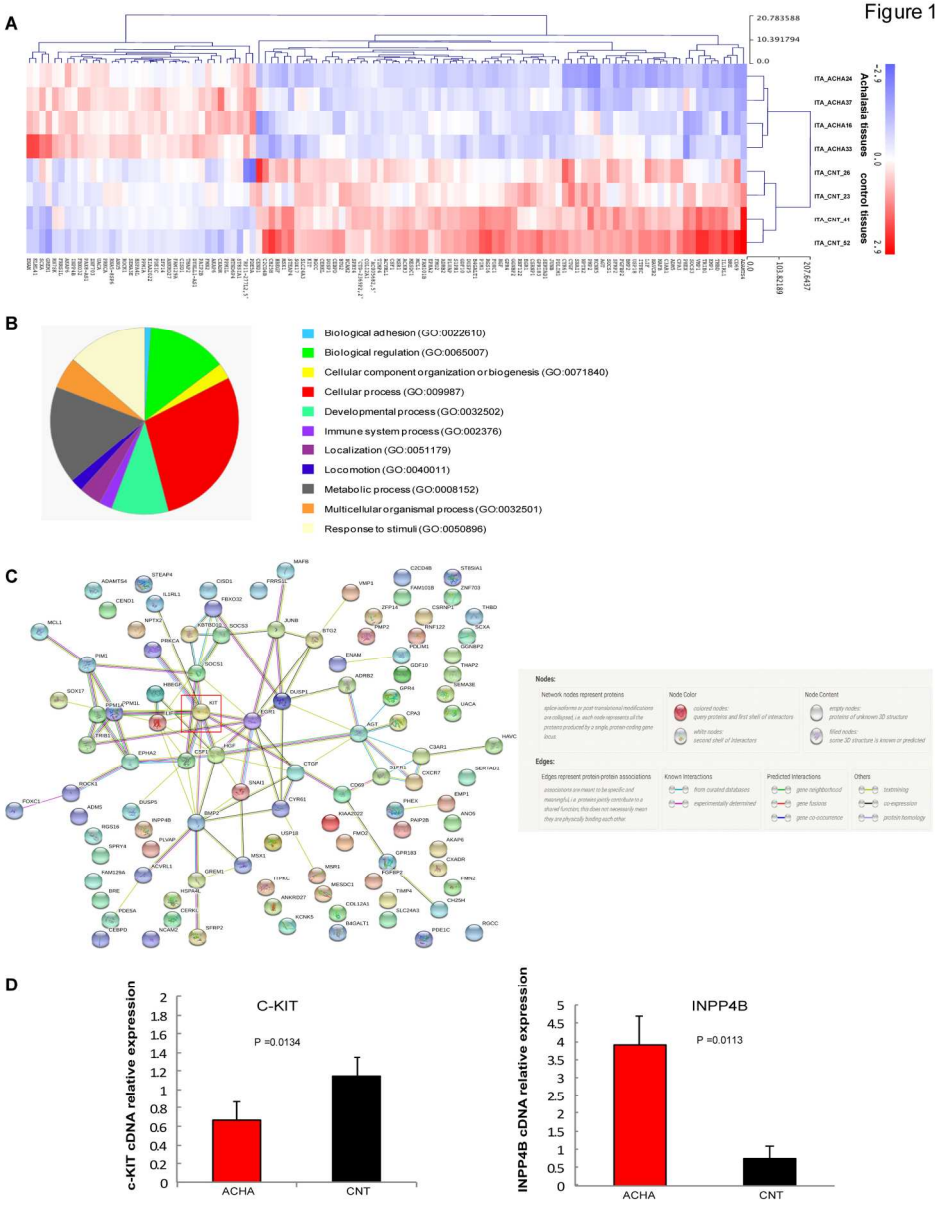


Figure 1. Differentially expressed genes in achalasia tissue. (A) Heat map showing the concordant differential expression observed in the tissues from achalasia patients compared to controls (for the genes reported in Table 1). Elaborated with MeV v4.8.1. (B) Biological processes of genes (GO-Slim Biological processes) differentially expressed in achalasia, as identified by PANTHER Functional Classification analysis. (C) Graphical output of significantly enriched protein-protein interactions determined with STRING analysis, showing the results of the 104 out of 111 dysregulated genes in achalasia, compared with data present in the STRING databases. The different colors in the figure inset identify the evidence for the different interactions (known; predicted; identified with other means, such as co-expression, data mining, and protein homology). The red square indicates c-KIT. (D) Real-time qRT-PCR data for c-KIT and INPP4B. Data from case and control tissue biopsies were normalized on a commercial pool of control tissue biopsies from esophagus. Student's t-test was performed and P values are indicated. Bars indicate standard deviations.

164x209mm (300 x 300 DPI)

1
2
3
4
5
6
7
8
9
10
11
12
13
14
15
16
17
18
19
20
21
22
23
24
25
26
27
28
29
30
31
32
33
34
35
36
37
38
39
40
41
42
43
44
45
46
47
48
49
50
51
52
53
54
55
56
57
58
59
60

For Peer Review

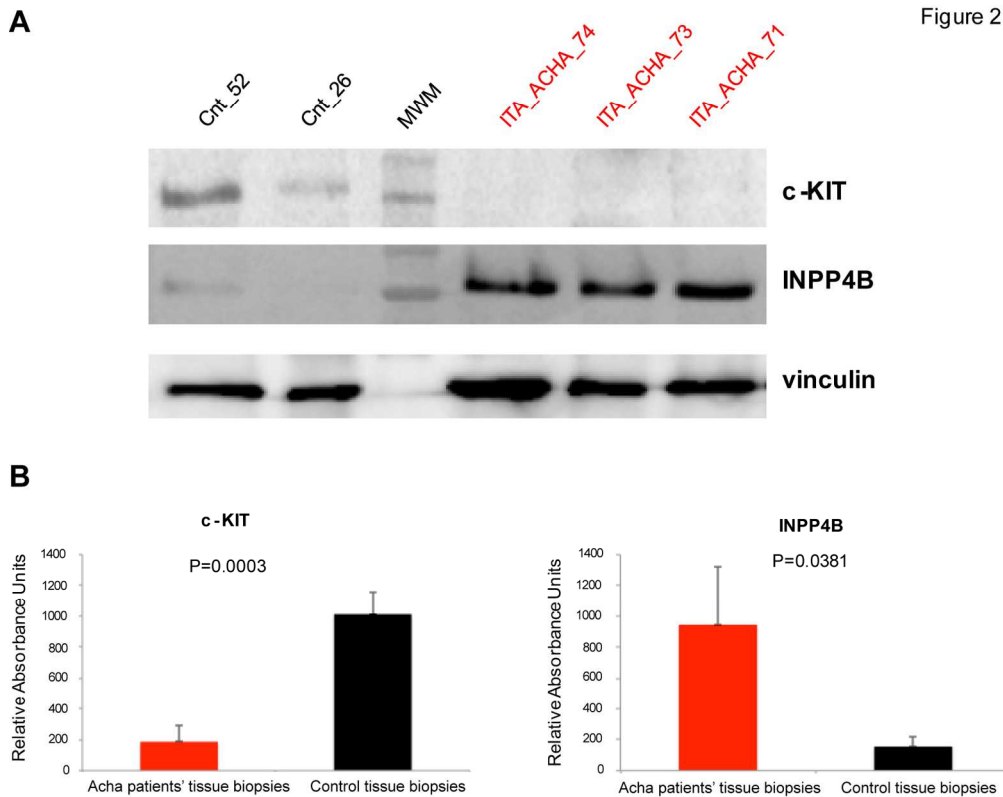


Figure 2. Western blot analysis of differentially expressed genes. (A) Example of the protein expression profiles in achalasia tissues compared to control samples for c-KIT and INPP4B. Western blotting was repeated in at least two independent experiments. (B) Densitometric analysis of the relative intensities for c-KIT and INPP4B. Quantitative data (mean values \pm standard deviation) from different experiments obtained from each individual were compared using Student's t-test for statistical analysis. For each sample, densitometric values were normalized on reference protein (vinculin). All experiments were carried out at least twice. Bars indicated standard deviations. P values are indicated in the graphs.

160x126mm (300 x 300 DPI)

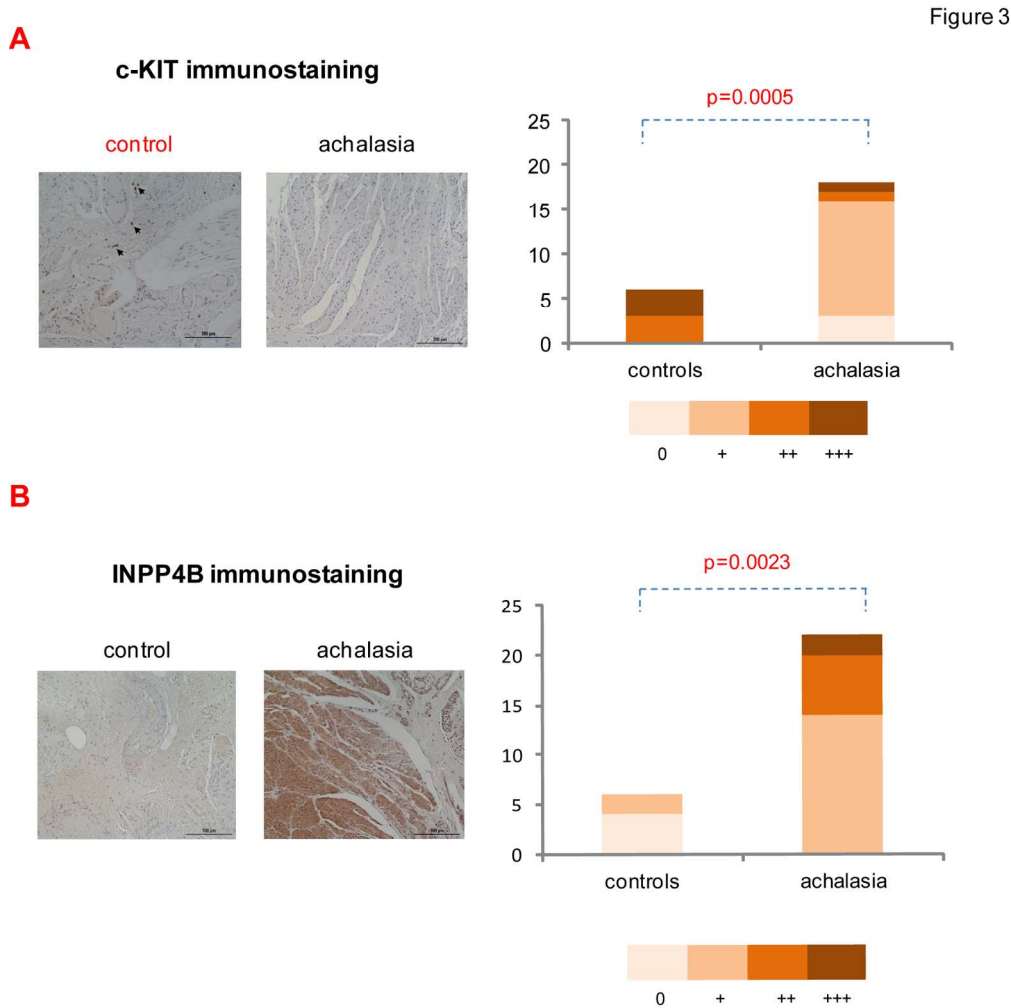


Figure 3. Immunostaining for c-KIT (A) and INPP4B (B). (A) Examples of the expression pattern for c-KIT in tissue biopsies from control (left) and achalasia patients (right). Arrows indicate the positive staining for c-KIT. c-KIT staining color histograms of controls (n=6) and cases (n=18) represent the number of samples assessed according to the semi-quantitative score. c-KIT immunolabeling differences in cases vs. controls were assessed by Fisher's exact test. (B) Examples of the expression pattern for INPP4B in tissue biopsies from control (left) and achalasia patients (right). INPP4B staining color histograms of controls (n=6) and cases (n=22) represent the number of samples assessed according to the semi-quantitative score. INPP4B immunolabeling differences in cases vs. controls were assessed by Fisher's exact test. Scale bars are 100µm as indicated.

159x160mm (300 x 300 DPI)

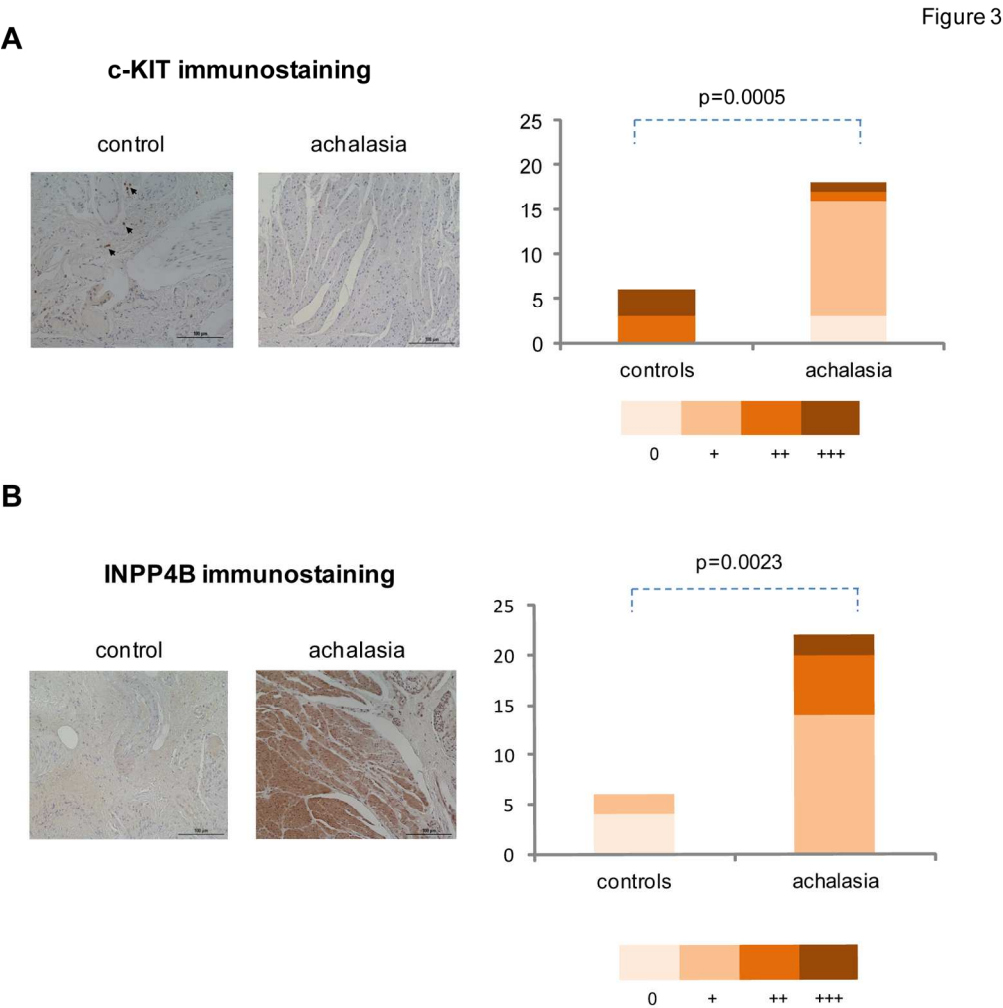


Figure 3. Immunostaining for c-KIT (A) and INPP4B (B). (A) Examples of the expression pattern for c-KIT in tissue biopsies from control (left) and achalasia patients (right). Arrows indicate the positive staining for c-KIT. c-KIT staining color histograms of controls (n=6) and cases (n=18) represent the number of samples assessed according to the semi-quantitative score. c-KIT immunolabeling differences in cases vs. controls were assessed by Fisher's exact test. (B) Examples of the expression pattern for INPP4B in tissue biopsies from control (left) and achalasia patients (right). INPP4B staining color histograms of controls (n=6) and cases (n=22) represent the number of samples assessed according to the semi-quantitative score. INPP4B immunolabeling differences in cases vs. controls were assessed by Fisher's exact test. Scale bars are 100µm as indicated.

159x160mm (300 x 300 DPI)

Figure 4

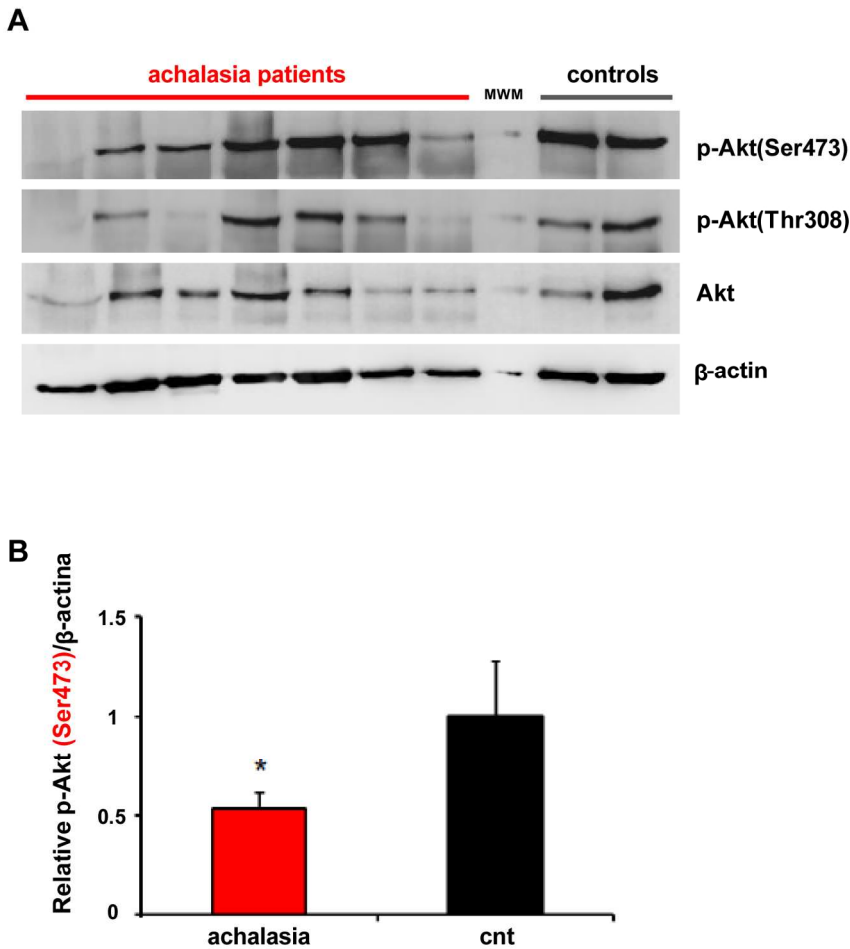


Figure 4. Phospho-Akt is down regulated in achalasia. (A) Example of the protein expression profiles in achalasia tissues compared to control samples of phospho-Akt (Ser473; Thr308) and total Akt. (B) Quantitative data (mean values ± standard deviation) from different experiments (performed in duplicate) obtained from each individual were compared using Student's t-test. For each sample, densitometric values were normalized on reference protein (β-actin). The significantly different relative phospho-Akt (Ser473) levels comparing achalasia vs. control tissues, were reported in the histogram (P=0.0495, Student's t-test). Bars indicate standard deviations.

159x154mm (300 x 300 DPI)

Figure 4

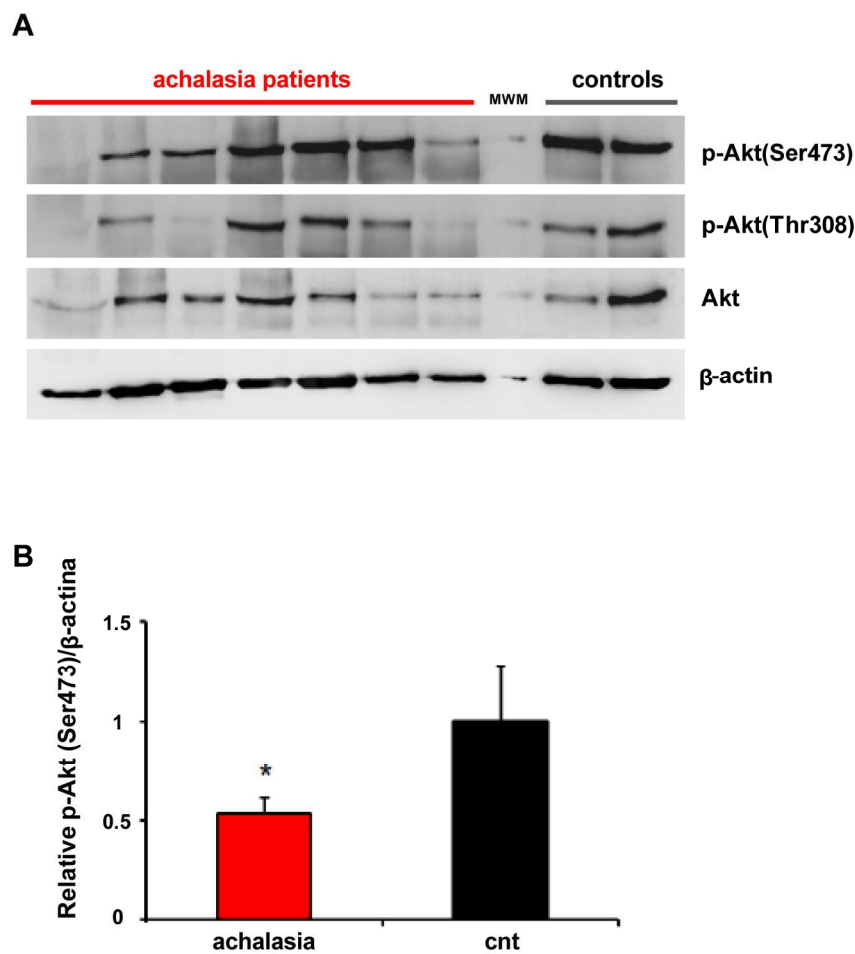


Figure 4. Phospho-Akt is down regulated in achalasia. (A) Example of the protein expression profiles in achalasia tissues compared to control samples of phospho-Akt (Ser473; Thr308) and total Akt. (B) Quantitative data (mean values \pm standard deviation) from different experiments (performed in duplicate) obtained from each individual were compared using Student's t-test. For each sample, densitometric values were normalized on reference protein (β -actin). The significantly different relative phospho-Akt (Ser473) levels comparing achalasia vs. control tissues, were reported in the histogram ($P=0.0495$, Student's t-test). Bars indicate standard deviations.

159x154mm (300 x 300 DPI)